

Combustion of Nano Aluminum Particles (Review)

D. S. Sundaram^a, V. Yang^a, and V. E. Zarko^{b,c}

UDC 536.46

Translated from *Fizika Goreniya i Vzryva*, Vol. 51, No. 2, pp. 37–64, March–April, 2015.
Original article submitted July 23, 2014; revision submitted October 8, 2014.

Abstract: Nano aluminum particles have received considerable attention in the combustion community; their physicochemical properties are quite favorable as compared with those of their micron-sized counterparts. The present work provides a comprehensive review of recent advances in the field of combustion of nano aluminum particles. The effect of the Knudsen number on heat and mass transfer properties of particles is first examined. Deficiencies of the currently available continuum models for combustion of nano aluminum particles are highlighted. Key physicochemical processes of particle combustion are identified and their respective time scales are compared to determine the combustion mechanisms for different particle sizes and pressures. Experimental data from several sources are gathered to elucidate the effect of the particle size on the flame temperature of aluminum particles. The flame structure and the combustion modes of aluminum particles are examined for wide ranges of pressures, particle sizes, and oxidizers. Key mechanisms that dictate the combustion behaviors are discussed. Measured burning times of nano aluminum particles are surveyed. The effects of the pressure, temperature, particle size, and type and concentration of the oxidizer on the burning time are discussed. A new correlation for the burning time of nano aluminum particles is established. Major outstanding issues to be addressed in the future work are identified.

Keywords: combustion, nanoparticles, aluminum, continuum, flame temperature, free-molecular heat transfer burning time, oxygen, combustion mechanism.

DOI: 10.1134/S0010508215020045

INTRODUCTION

Combustion of metal particles is of interest in various applications, including space [1, 2] and underwater propulsion [3], explosions [4], pyrotechnics [2], and hydrogen generation [5]. Among all elements of concern, boron has the highest volumetric heat of its reaction in oxygen, up to 138 kJ/cm³. Ignition of boron particles is, however, significantly delayed due to the presence of an oxide (B₂O₃) layer [6–8]. The ignition temperatures of boron particles in oxygenated environments are in the

range from 1500 to 1950 K, regardless of the particle size [7, 8]. Furthermore, energy release is significantly diminished in hydrogen-containing gases owing to the formation of meta-stable HBO₂ species [6]. Such difficulties of ignition and combustion of boron particles have so far limited the utilization of boron in practical applications. Beryllium is not widely used due to its extreme toxicity, relative scarcity, and high cost [9]. Aluminum, however, is the most abundant metal in the Earth's crust and is relatively safe to use [1]. One of the main issues in the combustion of micron-sized aluminum particles is their high ignition temperatures [10]. For particles with diameters greater than 100 μm, ignition is achieved only upon melting of the oxide (Al₂O₃) shell at 2350 K [10]. The molten oxide shell forms a cap due to the effects of surface tension and exposes the aluminum core, thereby allowing ignition of the particle.

^aSchool of Aerospace Engineering, Georgia Institute of Technology, Atlanta, GA, 30332, USA; vigor.yang@aerospace.gatech.edu.

^bVoevodsky Institute of Chemical Kinetics and Combustion, Siberian Branch, Russian Academy of Sciences, Novosibirsk, 630090 Russia.

^cResearch Institute of Applied Mathematics and Mechanics, Tomsk State University, Tomsk, 634050 Russia.

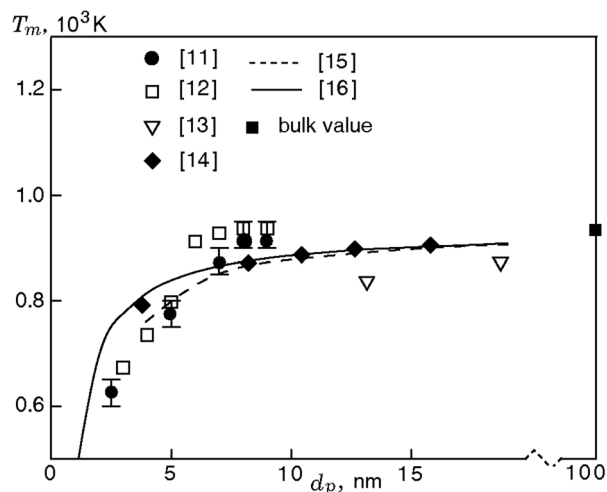


Fig. 1. Effect of the particle size on the melting temperature of nano aluminum particles [11].

The fraction of atoms in the surface layer of the particle increases dramatically as the particle size decreases below $1 \mu\text{m}$. It increases from 6 to 47% as the particle size decreases from 30 to 3 nm. The surface atoms have smaller coordination numbers and greater energies than the atoms in the interior regions of the particle. As a result, nano aluminum particles have unusual physicochemical properties compared with their micron-sized counterparts. Figure 1 shows the effect of the particle size on the melting temperatures of aluminum particles. The results of molecular dynamics (MD) simulations [11, 12], experiments [13, 14], and theoretical studies [15, 16] are shown in Fig. 1. The melting temperature T_m begins to deviate strongly from the bulk value (933 K) below $d_p < 10 \text{ nm}$ and attains a value of 673 K at about $d_p = 3 \text{ nm}$. There is a strong correlation between the melting temperature and the cohesive energy [17], which is the energy required to break a solid into a set of neutral free atoms. The cohesive energies of surface atoms are lower than those of interior atoms due to a smaller number of neighboring atoms. As the fraction of surface atoms in the particle increases with decreasing particle size, smaller particles melt at a lower temperature.

Figure 2 shows the effect of the particle size on the ignition temperature of aluminum particles T_{ign} [18–30]. The ignition temperature decreases with decreasing particle size, from 2350 K at $d_p = 100 \mu\text{m}$ to 933 K at $d_p = 100 \text{ nm}$. The oxide layer cracks due to tensile stresses exerted by the molten aluminum core [31] and/or polymorphic phase transformations in the oxide layer [30]. The aluminum core is then exposed to the oxidizing gas. The ensuing energy release results in

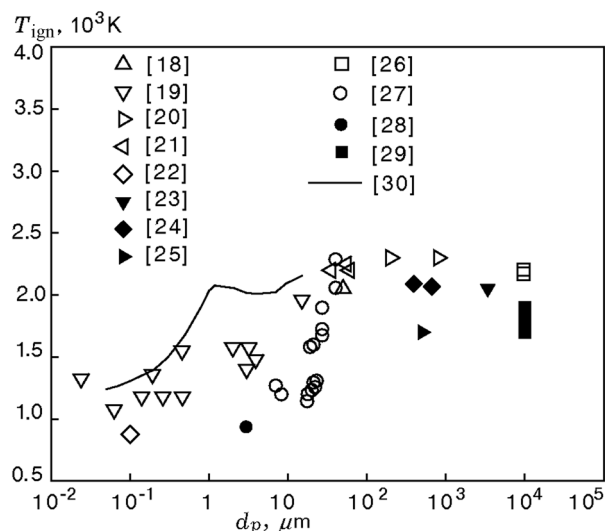


Fig. 2. Effect of the particle size on the ignition temperature of aluminum particles.

ignition of nano aluminum particles. For micron-sized particles, the energy release is insufficient to ignite the particles due to their higher volumetric heat capacity; ignition is only achieved upon melting of the oxide shell at 2350 K. Nevertheless, micron-sized aluminum particles ignite at significantly lower temperatures in water due to the formation of a weaker hydroxide layer [25] and/or stabilization of the γ -oxide polymorph [28]. For example, the ignition temperature of $3\text{-}\mu\text{m}$ particles in water is as low as 933 K [28]. The burning time of aluminum particles decreases by a factor of 4 as the particle size decreases from $10 \mu\text{m}$ to 100 nm [10]. Substantial enhancement in the burning properties can be obtained by substituting nano aluminum particles for micron-sized counterparts.

Nano aluminum particles have been used in a wide variety of combustion systems including nanofluids [32, 33], gelled propellants [34], solid propellants [35–38], and thermites [39–43]. Nanofluids are fluids in which nanoparticles are dispersed at very low concentrations ($<10 \text{ vol.}\%$). Tyagi et al. [32] explored the effects of nano-sized aluminum and aluminum oxide particles on the ignition characteristics of a diesel fuel over a temperature range of $688\text{--}768^\circ\text{C}$. Two different particle sizes of 15 and 50 nm were considered. The volume fraction of the particles varied in the range of $0\text{--}5\%$. The particle-laden droplets were dropped on a hot plate, and the ignition probability was calculated based on the number of droplets that ignited. The ignition probability of the diesel fuel was found to increase due to addition of nanoparticles. For example, at a temperature of 708°C , the ignition probability of the diesel fuel with

0.5 vol.% of nano aluminum particles is about 50%, which is greater than for a pure diesel fuel (15%). The enhancement of the ignition probability was attributed to the increase in the heat and mass transfer properties of the fuel.

Metallized gelled propellants are attractive for propulsion applications, because their energy densities are comparable to those of liquid systems [44]. Gels feature higher particle loading densities than nanofluids. Gelling reduces the risk of propellant leakages, but allows pumping and throttling. Gelled propellants are also less sensitive to the impact, friction, and electrostatic discharge than solid propellants and are not prone to cracking [44]. Nano aluminum particles act as a gelling agent due to their high specific surface area and can replace conventional inert gellants such as fumed silica. Sabourin et al. [34] measured the burning rates of gelled nitromethane with nano aluminum particles. The baseline particle size was 38 nm, and particle loading densities up to 15 wt.% were considered. The burning rate of pure nitromethane was positively affected by addition of nano aluminum particles. For example, at a pressure of 5 MPa, the burning rate increased by a factor of 4 as the particle loading density increased from 0 to 12.5%. This was primarily attributed to the enhancement in the energy content and thermal diffusivity of the mixture. The burning rate increased sharply at a loading density of $\approx 13\%$, and the resulting value was about an order of magnitude greater than the burning rate of pure nitromethane. The rapid increase in the burning rate corresponded to a change from a gel to clay-like consistency.

The burning behaviors of solid propellants with nano aluminum particles have also been studied with interest in the recent past. Meda et al. [36] measured the burning rates of solid propellants with 30- μm and 170-nm aluminum particles in a constant-pressure bomb over a pressure range of 1–70 atm. The propellant consisted of 17% of the HTPB binder, 68% of ammonium perchlorate, and 15% of aluminum by weight. The burning rate nearly doubled when nano aluminum particles were used instead of micron-sized counterparts. A qualitatively similar effect was also observed for thermites, which contain metal and metal oxide particles [45]. A novel energetic material consisting of nano aluminum particles and water is currently being explored for propulsion and energy-conversion applications [46–50]. This mixture is especially attractive due to its simplicity, low cost, and green exhaust products. The burning rates surpass those of many energetic materials, such as ammonium dinitramide (ADN) and hexanitrohexaazaisowurtzitane (CL-20). For example, at a pressure of 1 MPa, the burning rate of a stoichio-

metric 38-nm Al–H₂O mixture is 4.5 cm/s [46], which is nearly twice that of ADN [51].

Nano aluminum particles are covered by an inert oxide (Al₂O₃) layer 2–4 nm thick [46], which means that their active aluminum content is relatively low. For an oxide layer thickness of 3 nm, the mass fraction of the oxide layer increases with decreasing particle size, reaching a value of 52% at a particle size of 38 nm. The energy density of the particle is thus substantially diminished. Attempts to enhance the aluminum content have been marginally successful. For example, partial replacement of the aluminum oxide layer with a nickel coating increases the active aluminum content of nano aluminum particles by as much as 4% [52]. Alternative coating materials such as perfluoroalkyl carboxylic acids [53, 54], triphenylphosphine [55], and oleic and stearic acids [56] are also being considered to enhance the energetics of nano aluminum particles.

Nanoparticles pose serious safety issues during particle synthesis, handling, and storage. Nascent aluminum particles are inherently pyrophoric and can react with the oxidizing gas at room temperature. For 1- μm -sized and larger particles, the chemical reactions result in the formation of an oxide layer 2–4 nm thick. At nano scales, the energy release could be sufficient to ignite the particle due to its low volumetric heat capacity. The critical particle size below which aluminum particles are pyrophoric is 32 nm [57]. Therefore, great care must be taken when handling nano aluminum particles.

The objective of this paper is to review recent progress on combustion of nano aluminum particles and identify the major outstanding issues.

1. HEAT AND MASS TRANSFER REGIMES

1.1. Validity of the Continuum Assumption

Ignition and combustion of aluminum particles are typically studied by using continuum heat and mass transfer models [30, 58–60]. Two important length scales of concern are the particle diameter and the mean free path of the oxidizer molecules. The continuum assumption is valid if the mean free path of the gas molecules is substantially smaller than the particle diameter. At nano scales, the particle diameter is comparable to or even smaller than the mean free path. The particle behaves like a large molecule, and the gas cannot be treated as a continuum medium. It is commonly accepted that the continuum assumption breaks down for Knudsen numbers $\text{Kn} > 0.01$, and the free-molecular regime prevails for $\text{Kn} > 10$ [61, 62]. The Knudsen num-

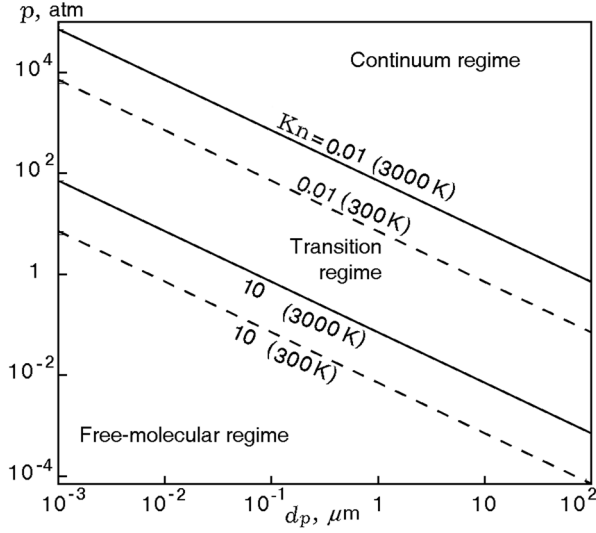


Fig. 3. Critical particle size for the transition from the continuum to the free-molecular regime as a function of pressure for two different temperatures: 300 and 3000 K.

ber is the ratio of the mean free path to the particle size [63]

$$\text{Kn} = \frac{RT}{\sqrt{2}\pi d_a^2 N_A p d_p}, \quad (1)$$

where R is the universal gas constant, T is the temperature, d_a is the diameter of the ambient gas molecule, N_A is the Avogadro number, p is the pressure, and d_p is the particle diameter.

The transition regime concerns intermediate Knudsen numbers in the range from 0.01 to 10. Figure 3 shows the particle sizes corresponding to Knudsen numbers of 0.01 and 10 as a function of the pressure p for two different temperatures of 300 and 3000 K. At a pressure of 1 atm and combustion temperature of 3000 K, the particle size at which the continuum approximation ceases to be valid is 70 μm . It decreases by a factor of 10 as the pressure increases from 1 to 10 atm and the temperature decreases from 3000 to 300 K. Continuum models fail to give accurate predictions of the heat and mass transfer processes for nano aluminum particles.

1.2. Heat and Mass Transfer Rates at Nano Scales

The rates of heat transfer between the particle and gas in the continuum (\dot{Q}_{cont}) and free-molecular (\dot{Q}_{free}) regimes are given by the following formulas [64]:

$$\dot{Q}_{\text{cont}} = 2\pi d_p \lambda_a (T_p - T_a), \quad \text{Kn} < 0.01, \quad (2)$$

$$\dot{Q}_{\text{free}} = \alpha \pi d_p^2 \frac{p_a}{8} \sqrt{\frac{8k_B T_a}{\pi m_a}} \left(\frac{\gamma + 1}{\gamma - 1} \right) \left(\frac{T_p}{T_a} - 1 \right), \quad \text{Kn} > 10. \quad (3)$$

Here λ is the thermal conductivity, α is the energy accommodation coefficient (the ratio of the actual average energy transferred during a collision to the theoretical value under complete energy accommodation), k_B is the Boltzmann constant, m_a is the average mass of the gas molecule, and γ is the ratio of specific heats. The subscripts a and p denote the ambient gas and particle, respectively.

In the continuum regime, the heat transfer rate is linearly proportional to the particle size and depends on the thermal conductivity of the gas. This is because collisions between gas molecules control the rate of heat transfer between the particles and the gas. In the free-molecular regime, the heat transfer rate is dictated by collisions of gas molecules on the particle surface. Consequently, it is strongly dependent on the particle surface area, energy accommodation coefficient, molecular speed, and gas pressure. Note that a closed-form expression for the heat transfer rate cannot be obtained for particles in the transition regime, and a numerical analysis is required [62].

The mass flow rate of the oxidizer to the particle surface is also a function of the Knudsen number. For diffusion-controlled conditions, the following expressions for the particle mass consumption rate are obtained by enforcing continuity of the mass flow rate of the oxidizer [44, 65]:

$$\dot{m}_{p,\text{cont}} = 2\pi d_p \rho_a D_{\text{ox}} \log(1 + iY_{\text{ox},a}), \quad \text{Kn} < 0.01, \quad (4)$$

$$\dot{m}_{p,\text{free}} = d_p^2 p_a Y_{\text{ox},a} M_a i \sqrt{\frac{\pi}{2RT_a M_{\text{ox}}}}, \quad \text{Kn} > 10. \quad (5)$$

Here ρ is the density, D is the diffusivity, i is the stoichiometric fuel-oxidizer mass ratio, Y is the mass fraction, and M is the molecular weight. The subscript “ox” refers to the oxidizer.

In the continuum regime, the particle mass burning rate is independent of pressure, since the pressure effects on diffusivity and density cancel each other. The mass burning rate is, however, linearly proportional to pressure in the free-molecular regime. Figure 4 shows the effect of the particle size on the heat transfer rate \dot{Q} and particle mass burning rate \dot{m}_p in the continuum and free-molecular regimes. The temperatures of the particle and the gas are taken to be 300 and 1000 K, respectively. Continuum models substantially overestimate the heat and mass transfer rates at nano scales.

An implicit assumption in the previous analysis is that the particle is not vaporizing and reactions occur on the particle surface. For vaporizing particles, the particle mass burning rate takes the following form [44]:

$$\dot{m}_{p,\text{cont}} = 2\pi d_p \rho_a D_{\text{ox}} \times \log \left(1 + \frac{iY_{\text{ox},a} H_r + c_p (T_a - T_s)}{L_v} \right). \quad (6)$$

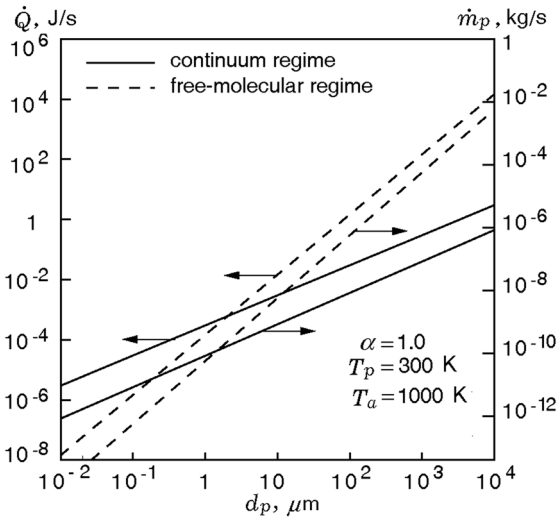


Fig. 4. Effect of the particle size on the heat transfer rate and the particle mass burning rate in the continuum and free-molecular regimes.

Here H_r is the reaction heat, c_p is the specific heat, and L_v is the latent heat of vaporization.

The mass burning rate of a vaporizing particle is nearly twice the counterpart of a condensed-phase particle.

1.3. Deficiencies of Continuum Models

Recent works have highlighted the deficiencies of continuum models in predicting the ignition properties of nano aluminum particles. Sundaram et al. [57] studied pyrophoricity of nano aluminum particles in air at a pressure of 1 atm, based on a transient energy balance analysis. The study considered conduction and radiation heat losses to the ambient gas. The heterogeneous oxidation process was modeled by means of the Mott–Cabrera kinetic theory. Based on a free-molecular heat transfer model, nascent aluminum particles smaller than 32 nm were predicted to be pyrophoric. Reasonably good agreement with experimental data was achieved [57]. The continuum model, however, significantly overestimated heat losses to the ambient gas; the resulting critical particle size was 18 nm.

A similar analysis was conducted to investigate the ignition delay of metal nanoparticles in air at a pressure of 1 atm [62]. The particle size range of concern was 10 nm to 50 μm . The study was also based on a transient energy balance analysis and considered heat losses to the ambient gas. An Arrhenius-type reaction rate model was employed to model particle oxidation. The initial temperatures of the particles and the gas were taken to be 300 and 2000 K, respectively. The ignition delay of nanoparticles turned out to be lin-

early proportional to the particle size, in contrast to the quadratic size dependence observed for micron-sized particles. This was attributed to the transition from the continuum to the free-molecular heat transfer regime as the particle size decreased from micron to nano scales. Experimental data also suggested that the ignition delay of nano aluminum particles was only weakly dependent on the particle size [19]. For example, the ignition delay decreased only by a factor of about 2 as the particle size decreased from 1 μm to 100 nm. For micron-sized aluminum particles, the ignition delay quadrupled as the particle size was doubled [58]. Further studies are necessary to understand why the actual particle size effect on the ignition delay is weaker than the predictions of the models.

The free-molecular regime is prevalent during combustion of nano aluminum particles. The adiabatic flame temperature of aluminum particles in oxygenated environments is as high as 4000 K. At such high temperatures, the mean free path is about an order of magnitude greater than the particle size. Allen et al. [66] conducted a transient energy balance analysis and calculated the flame temperature and the burning time of 80-nm aluminum particles in an oxygen–nitrogen gas mixture at a pressure of 20 atm and a temperature of 1500 K. The molar concentration of oxygen in the gas was 20%. The reaction rate was assumed to be controlled by collisions of gas molecules on the particle surface. Shock tube experiments were also performed under similar conditions; the flame temperature and the burning time were inferred by monitoring the intensity of light emitted by the particles. The measured flame temperature of 80-nm particles was about 3200 K and the burning time was on the order of 100 μs at a pressure of 20 atm [66]. The continuum heat transfer model underpredicted the burning time approximately by three orders of magnitude. Reasonable agreement with experimental data was achieved by using the free-molecular heat transfer model only.

Ermoline et al. [65] developed a theoretical model of heterogeneous combustion of metal particles in the transition heat and mass transfer regime. The analysis considered the mass and energy balances for the particle and gas phases. The particle was assumed to be non-volatile, and the burning rate was dictated by diffusion of the oxidizing gas to the particle surface. To facilitate comparisons with experimental measurements, the model was employed to calculate the burning times of zirconium particles in air at a pressure of 1 atm. Qualitatively similar results were expected for aluminum particles. The particle size range of concern was 1–200 μm . For particles smaller than 10 μm , deviations from the classical d^2 law became significant, and

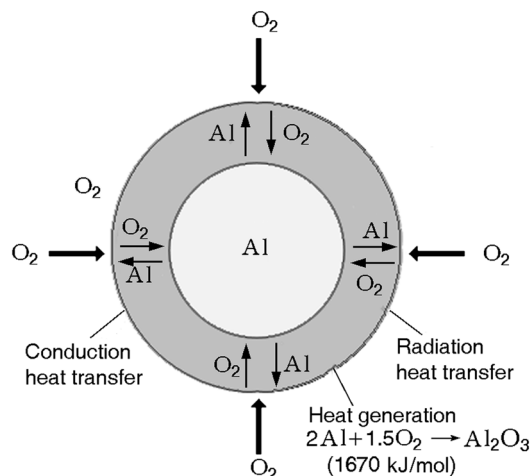


Fig. 5. Key physicochemical processes in combustion of nano aluminum particles in oxygen.

the burning time was linearly dependent on the particle size. This is in qualitative agreement with experimental data. Note that continuum models suggest that the burning time should be quadratically proportional to the particle size, which contradicts experimental observations. The disparity between the predictions and experimental data was attributed to the effect of finite-rate kinetics. It is apparent that continuum models fail to accurately predict the ignition and combustion properties of nano aluminum particles.

2. PARTICLE COMBUSTION MECHANISMS

Combustion of nano aluminum particles involves an array of physicochemical processes such as heat and mass transfer between the particle and the gas, phase transformations in the oxide layer, and exothermic chemical reactions. Figure 5 shows the key phenomena during combustion of nano aluminum particles in oxygen. The particles are covered by an oxide (Al_2O_3) layer 2–4 nm thick [46]. Combustion of nano aluminum particles occurs heterogeneously on the particle surface. The oxidizer gas molecules diffuse toward the particle surface and react with aluminum atoms. The ensuing energy release heats up the particles and the heat is transferred to the ambient gas by conduction and radiation. The three important processes that typically control the burning rate are: (1) mass diffusion through the gas-phase mixture; (2) mass diffusion across the oxide layer of the particle; (3) chemical reactions [67].

2.1. Mass Diffusion through the Gas-Phase Mixture

For diffusion-controlled conditions, the reaction rate is much faster than the rate of diffusion of reactant species. The particle burning rate is dictated by the mass flow rate of the reactants. Equations (4) and (5) are integrated to obtain closed-form expressions for the burning time of aluminum particles:

$$t_{b,\text{diff,cont}} = \frac{\rho_p d_p^2}{8\rho_a D_{\text{ox}} \log(1 + iY_{\text{ox},a})}, \quad \text{Kn} < 0.01, \quad (7)$$

$$t_{b,\text{diff,free}} = \frac{\rho_p d_p}{ip_a Y_{\text{ox},a} M_a} \sqrt{\frac{\pi R T_a M_{\text{ox}}}{2}}, \quad \text{Kn} > 10. \quad (8)$$

In the continuum regime, the burning time is quadratically proportional to the particle size and is independent of the gas pressure, because the pressure effects of density and diffusivity cancel each other. In the free-molecular regime, the burning time is linearly dependent on the particle size and is inversely proportional to pressure. For temperatures of concern (≈ 3000 K), the continuum assumption is valid for particles larger than $\approx 70 \mu\text{m}$ at a pressure of 1 atm. The free-molecular regime prevails for particles smaller than 100 nm. For intermediate particle sizes, closed-form expressions for the burning time are not available.

The diffusion coefficient of oxygen in air is given by [68]

$$D_{\text{ox}} = k_1 \left(\frac{T}{T_0} \right)^{k_2} \frac{p_0}{p}, \quad (9)$$

where T [K] is the temperature, p [atm] is the pressure, T_0 is the reference temperature (1 K), and p_0 is the reference pressure (1 atm). The constants are $k_1 = 1.13 \cdot 10^{-9} \text{ m}^2/\text{s}$ and $k_2 = 1.724$, respectively.

The resulting burning time of 80-nm aluminum particles is on the order of 10^{-8} to 10^{-7} s at a pressure of 8 atm. Bazyn et al. [69] measured the burning times of 80-nm aluminum particles in a shock tube in oxygen–nitrogen gas mixtures at two different pressures of 8 and 32 atm and over a temperature range of 1200–2200 K. The burning time was obtained by monitoring the temporal variations of the intensity of the visible light emitted by the particle. The time period between 10% and 90% of the total integrated intensity was taken as the burning time. The measured burning times are on the order of 10^{-4} s, orders of magnitude greater than the theoretical counterparts for diffusion-controlled conditions. It is likely that mass diffusion through the gas-phase mixture does not control the burning rate of nano aluminum particles.

2.2. Mass Diffusion across the Oxide Layer

If mass diffusion across the oxide layer of the particle is the rate-controlling process, the burning time can be expressed as [70]

$$t_b = \frac{\rho_p d_p^2}{32D_1 C_{\text{ox},a}}, \quad (10)$$

where $C_{\text{ox},a}$ is the molar concentration of oxygen in the gas and D_1 is the oxygen diffusion coefficient through the oxide layer, which is not a well-known quantity.

Henz et al. [71] conducted molecular dynamics simulations of mechanochemical behaviors of nano aluminum particles of diameters 5.6 and 8.0 nm. Two different oxide layer thicknesses of 1 and 2 nm were considered. The particles were heated from 300 to 3000 K at a heating rate of 10^{12} K/s. Particle oxidation was characterized by the species diffusion process. The mass diffusivity in the oxide layer was 10^{-9} to 10^{-7} m²/s over the temperature range of 1000–2000 K. With the diffusion coefficients being substituted into Eq. (10), the burning times were calculated to be 10^{-6} to 10^{-4} s, which were comparable to the measured burning times of $\approx 10^{-4}$ s. Note that MD simulations did not treat the presence of defects in the oxide layer. In reality, defects facilitate cracking of the oxide layer upon core melting and/or polymorphic phase transformations in the oxide layer [30, 31]. The existing cracks heal upon oxidation, whereas new cracks are continuously created. It is thus possible that the oxide layer offers negligible diffusion resistance during combustion of nano aluminum particles. Further studies are necessary to fully understand the role of the oxide layer in particle combustion.

Mass diffusion across the oxide layer is of paramount concern at temperatures lower than the core melting point (933 K) and/or low heating rates ($<10^3$ K/s). Park et al. [70] studied the oxidation of nano aluminum particles by using a single particle mass spectrometer (SPMS) for temperatures up to 1373 K at low heating rates ($<10^3$ K/s). The particle size range of concern was 50–150 nm. The particles did not burn completely. For example, at a temperature of 1373 K, only about 40% of the particle mass oxidized after 15 s of its heating. Experimental data suggests that particle oxidation was controlled by species diffusion across the oxide layers of the particles. These observations contradict those of Bazyn et al. [69], which were obtained at higher heating rates (10^6 – 10^8 K/s) and temperatures (1200–2200 K) in a shock tube. The measured burning times of 80-nm particles were on the order of $\approx 10^{-4}$ s, orders of magnitude smaller than those obtained by Park et al. [70]. It is likely that the study

of Park et al. [70] dealt with reactions preceding ignition, while Bazyn et al. [69] treated combustion of nano aluminum particles. Eisenreich et al. [72] also investigated the mechanism of low-temperature oxidation of passivated nano and micron-sized aluminum particles by using a thermogravimetric analysis. The particle size varied between 100 nm to 25 μm . The initial oxide-layer thickness based on the weight gain of the particles due to chemical reactions (oxidation) was estimated as 3.6 nm. A two-stage behavior was observed during particle heating. The first step was the buildup of an oxide layer 6–10 nm thick, which was dictated by chemical kinetics. The second step was much slower and involved both mass diffusion through the oxide layer and chemical reactions.

Aita et al. [73] developed a theoretical model of combustion of nano aluminum particles in pure oxygen. The burning rate was assumed to be controlled by mass diffusion across the oxide layer. The results suggested that the burning time should be quadratically proportional to the particle size, which contradicts experimental data. In reality, the particle size exerts a much weaker effect on the burning time; the exponent of the burning time curve as a function of the particle diameter is significantly smaller than unity. This appears to support the idea that mass diffusion across the oxide layer is not the rate-controlling process in combustion of nano aluminum particles.

2.3. Chemical Kinetics

It is likely that chemical kinetics controls the burning rate of nano aluminum particles. Empirical evidence that support this hypothesis will be presented in Section 4.3. For kinetically controlled conditions, the rate of diffusion of the reactant species is much faster than chemical kinetics. The mass burning rate of the particles takes the form [44]

$$\dot{m}_{b,\text{chem}} = \pi d_p^2 M_{\text{Al}} k p_a X_{\text{ox},a} \quad [\text{g/s}], \quad (11)$$

where k is the reaction rate constant, M_{Al} is the molecular weight of aluminum, and $X_{\text{ox},a}$ is the molar fraction.

Equation (11) can be integrated to obtain a closed-form expression for the burning time under kinetically controlled conditions:

$$t_{b,\text{chem}} = \frac{\rho_p d_p}{2M_{\text{Al}} k p_a X_{\text{ox},a}}. \quad (12)$$

The reaction rate constant takes the form

$$k = A \exp\left(-\frac{E_a}{RT}\right), \quad (13)$$

where A is the pre-exponential constant and E_a is the activation energy.

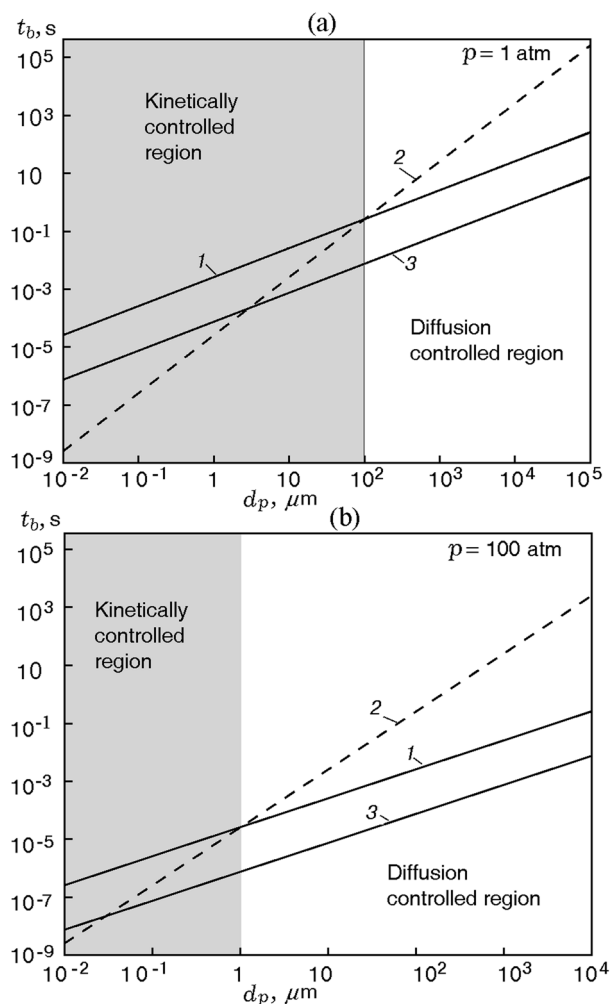


Fig. 6. Comparison of the aluminum particle burning times in air under diffusion-controlled and kinetically controlled conditions at pressures of 1 and 100 atm: curves 1 show the effect of chemical kinetics (at 3000 K); curves 2 and 3 show the effect of diffusion in the continuum (2) and free-molecular (3) regimes.

For kinetically controlled conditions, the burning time is linearly proportional to the particle size and is a strong function of the pressure and temperature of the ambient gas. The chemical rate constants can be obtained from experimental data of Bazyn et al. [69]. The particle size is 80 nm, and the gas consists of oxygen and nitrogen (both with the molar fractions of 50%). The activation energy is obtained by fitting the burning time versus temperature curves. At the pressure $p = 8$ atm, the activation energy is 71.6 kJ/mol and the burning time is 0.29 ms at 1400 K [69]. With these values being substituted into Eqs. (12) and (13), the pre-exponential constant is estimated to be 1618.5 mol/(m²·s·atm).

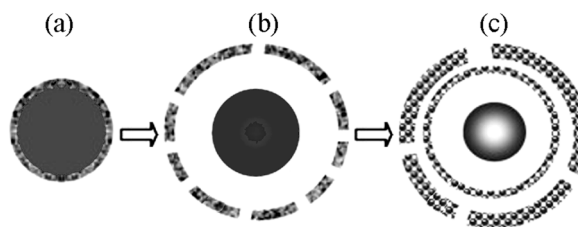


Fig. 7. Schematic of the melt-dispersion mechanism of combustion of nano aluminum particles at a high heating rate ($>10^6$ K/s) [74]: (a) aluminum core covered by the initial alumina shell; (b) fast melting of aluminum leads to spallation of the alumina shell; (c) unloading wave propagates to the center of the molten core of the Al particle and generates tensile pressure, which disperses small Al clusters.

The diffusion and chemistry times can be compared to ascertain the critical particle size at which the transition from diffusion-controlled to kinetically controlled conditions occurs. Figure 6 shows the particle burning times under diffusion-controlled and kinetically controlled conditions at pressures of 1 and 100 atm. Mass diffusion is faster than chemical reactions for particle diameters smaller than the critical value, which is 100 μm at $p = 1$ atm. The burning rate of particles larger than 100 μm is controlled by the mass diffusion process. The critical particle size decreases from 100 to 1 μm as the pressure increases 1 to 100 atm. The analysis suggests that combustion of nano aluminum particles is kinetically controlled over the pressure range of concern (1–100 atm).

2.4. Alternative Mechanisms

Alternative theories have been proposed to explain the combustion mechanism of nano aluminum particles. Levitas et al. [74, 75] proposed the melt-dispersion mechanism, which becomes operative at high heating rates ($>10^6$ K/s). Figure 7 shows the schematic of the melt-dispersion mechanism for nano aluminum particles. Melting of the aluminum core creates pressures of 1–4 GPa, which causes spallation of the oxide shell. The ensuing pressure imbalance between the core and the exposed surface results in an unloading wave and disperses small liquid aluminum clusters. The liquid aluminum clusters react with the oxidizing gas. Lynch et al. [76] employed absorption spectroscopy to detect the presence of the aluminum vapor for 80-nm aluminum particles in argon with the help of a shock tube. The pressure of the ambient gas was 7 atm. The gas temperature was decreased from 3000 K in increments of about 100 K until the aluminum vapor was not seen in the absorption spectrum. The aluminum vapor was not present at temperatures lower than 2275 K. If aluminum

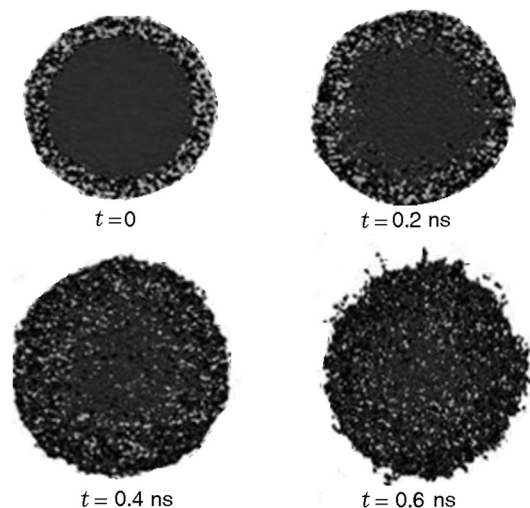


Fig. 8. Snapshots of the central slice of a 26-nm aluminum particle covered by an oxide (Al_2O_3) shell 3 nm thick: the images are obtained by means of molecular dynamics simulations; the snapshots show core Al atoms (black points), shell Al atoms (dark gray points), and shell O atoms (light gray points).

clusters were present, the measurements would have detected the aluminum vapor corresponding to the equilibrium partial pressure. This suggests that spallation of the oxide layer and dispersion of aluminum clusters do not occur upon melting of the aluminum core [76]. Further studies are necessary to shed light on the melt-dispersion mechanism for nano aluminum particles.

Molecular dynamics simulations provide a detailed insight into the combustion mechanisms of nano aluminum particles. Li et al. [77, 78] conducted MD simulations of combustion of nano aluminum particles for three different particle sizes of 26, 36, and 46 nm. The oxide layer thickness was taken as 3 nm. Ignition was achieved by heating the particles to a temperature of 1100 K. Figure 8 shows the snapshots of the central slice of a 26-nm aluminum particle at various times. Aluminum atoms of the core reacted with oxygen atoms of the shell, thereby heating the particle beyond the melting temperature of the shell. Shattering and fragmentation of the shell were not observed. Melting of the shell was followed by ejection of aluminum atoms into the ambient gas. The onset temperature of ejection is independent of the particle size, whereas the onset instant and the time delay to the peak rate of temperature changing decrease with decreasing particle size. This is consistent with the fact that the reactivity of the particle increases with decreasing particle size, but empirical evidence that would support the proposed mechanism is yet to be found.

Table 1. Thermophysical properties of aluminum and aluminum oxide

Property	Value
$T_{m,\text{Al}}$, K	933
$T_{\text{boil,Al}}$, K*	2791
$T_{m,\text{ox}}$, K	2350
$T_{\text{boil,ox}}$, K*	4000
$\Delta H_{f,\text{ox}}$, kJ/mol**	-1676
$H_{T_{\text{boil,ox}}} - H_{298} + \Delta H_{\text{boil,ox}}$, kJ/mol	2550

Notes: *1 atm; **298 K.

3. MODES OF COMBUSTION AND FLAME STRUCTURES

3.1. Gas-Phase versus Surface Combustion

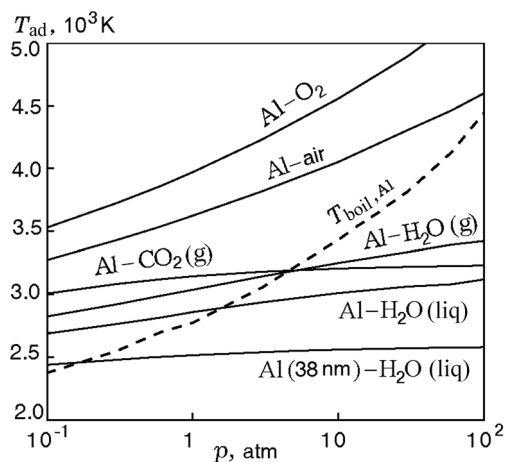
Aluminum particles can undergo gas-phase or surface reactions, depending on the particle size, pressure, and type of the oxidizing gas. Table 1 shows the properties of aluminum and aluminum oxide. The melting and boiling temperatures of aluminum are lower than those of aluminum oxide. For example, at a pressure of 1 atm, the boiling temperatures of aluminum and aluminum oxide are 2791 and 4000 K, respectively. The heat of formation of aluminum oxide is lower than the amount of energy required to heat the oxide to its boiling temperature and vaporize the oxide. Consequently, the adiabatic flame temperature of aluminum particles in pure oxygen cannot exceed the boiling temperature of the oxide. The possibility of gas-phase combustion exists because the boiling temperature of aluminum is lower than that of the oxide [79, 80]. Table 2 shows the adiabatic flame temperatures and reaction products for aluminum particles in different oxidizers at the pressure $p = 1$ atm. The calculations were performed by using the NASA Chemical Equilibrium with Applications (CEA) program [81]. In most cases, the adiabatic flame temperature is lower than the boiling temperature of the oxide (4000 K). An exception is the Al- F_2 system, which is characterized by a flame temperature of ≈ 4400 K. Combustion of aluminum particles in fluorine is similar to burning of hydrocarbon droplets due to sublimation of AlF_3 . Except for the carbon monoxide, the adiabatic flame temperatures are greater than the boiling temperature of aluminum. Gas-phase reactions are, thus, expected for most oxidizers at $p = 1$ atm.

The gas pressure exerts a significant effect on the mode of combustion of aluminum particles. Figure 9 shows the effect of pressure on the adiabatic flame temperature of aluminum particles for different oxidizers

Table 2. Adiabatic flame temperature and product composition for combustion of aluminum with different oxidizers at 1 atm

Reactants	T_{ad} , K	Products (molar concentration above 1%)
2Al(s) + 1.5O ₂	3977.0	Al, AlO, Al ₂ O, Al ₂ O ₂ , O, O ₂ , Al ₂ O ₃ (liq)
2Al(s) + 1.5(O ₂ + 3.76Ar)	3624.8	Al, AlO, Al ₂ O, Ar, O, O ₂ , Al ₂ O ₃ (liq)
2Al(s) + 1.5(O ₂ + 3.76N ₂)	3546.5	Al, AlO, Al ₂ O, NO, N ₂ , O, Al ₂ O ₃ (liq)
2Al(s) + 3N ₂ O	3746.9	Al, AlO, Al ₂ O, Al ₂ O ₂ , NO, N ₂ , O, O ₂ , Al ₂ O ₃ (liq)
2Al(s) + 3H ₂ O	3052.8	H, H ₂ , H ₂ O, AlOH, Al ₂ O ₃ (liq)
2Al(s) + 3CO ₂	3144.4	CO, CO ₂ , Al ₂ O ₃ (liq)
2Al(s) + 3CO	2277.2	Al, Al ₂ O, CO, Al ₄ C ₃ , Al ₂ O ₃ (a), C(gr)
2Al(s) + 1.5F ₂	4414.5	Al, AlF, AlF ₂ , F
2Al(s) + 1.5(F ₂ + 3.76Ar)	3873.5	AlF, AlF ₂ , AlF ₃ , Ar, F

Note: The solid, liquid, amorphous, and graphite states are indicated by s, liq, a, and gr, respectively.

**Fig. 9.** Effect of pressure on the adiabatic flame temperature for different oxidizers and particle sizes.

and particle sizes under stoichiometric conditions. The flame temperature is lower than the boiling temperature of aluminum for pressures over a threshold value. The threshold pressure is around 2, 5, and 100 atm for water vapor, carbon dioxide, and air, respectively. Surface reactions are, thus, more important for oxidizers such as water and carbon dioxide, especially at higher pressures. The particle size may also affect the mode of combustion at a given pressure. For example, the cut-off pressure decreases from ≈ 2.0 to 0.2 atm as the particle size decreases from 1 μm to 38 nm. This can be attributed to the fact that the inert oxide layer constitutes a greater portion of the particle mass at nano scales; a 38-nm aluminum particle, for example, contains 47 wt.% of the oxide [46]. The adiabatic flame temperature in water decreases by about 500 K as the

particle size decreases from 1 μm to 38 nm. Combustion of nano aluminum particles in liquid water must, therefore, occur heterogeneously on the particle surface over the pressure range of practical concern (1–100 atm).

For micron-sized and larger particles, numerous experimental studies substantiate the fact that gas-phase reactions occur in oxygen-containing gases [82–85], whereas surface reactions are more prominent in water and carbon dioxide [84, 86, 87]. Yetter and Dryer [84] studied combustion of a 210- μm aluminum particle burning in air, carbon dioxide, and water vapor at 1 atm. The particles were ignited by a laser and fell under the effect of gravity. The presence of a detached diffusion flame in air implies that reactions occur away from the particle surface. This is consistent with the results of the chemical equilibrium analysis. Planar laser-induced fluorescence (PLIF) and electron probe microanalysis (EPMA) were used to measure the profiles of temperature and species concentrations. Peak concentrations of AlO and Al₂O₃ were at $d_f/d_p = 2.0$ –2.8 and $d_f/d_p = 2.4$ –3.5, respectively. The temperature attained its maximum value of 3800 K at $d_f/d_p = 5.0$ –6.0. The measured peak temperature is approximately equal to the adiabatic flame temperature of the aluminum–air system at 1 atm (≈ 3500 K). A similar result was obtained by Dreizin [88] for 90- μm and 250- μm aluminum particles burning in oxygenated environments at a pressure of 1 atm. For oxygen concentrations greater than 10%, the flame temperature was 3273 K.

The concentration of the oxidizer in the gas is an important parameter that dictates the flame standoff distance. Wilson and Williams [85] studied combustion of 50- μm aluminum particles in oxygen–argon gas mixtures. The particles were ignited by a focused laser

beam and observed by cinephotomicrography throughout the entire burning history. The flame diameter was inferred by monitoring the extremes in the radial intensity distribution. The measured flame standoff ratio (d_f/d_p) increased from 2.8 to 5.9 as the oxidizer concentration increased from 10 to 50%. This further corroborates the fact that gas-phase reactions occur for micron-sized aluminum particles in oxygen-containing gases.

Surface reactions are more important for such oxidizers as carbon dioxide and water vapor. For carbon dioxide, the measured flame temperature (≈ 3200 K) is approximately equal to the adiabatic counterpart [89, 90]. The peak concentration of AlO takes place at $d_f/d_p = 1.3$. The flame standoff ratio is as low as ≈ 1.5 in water-vapor-containing environments [91].

Legrand et al. [86] investigated combustion of 60- μm aluminum particles in carbon dioxide over a pressure range of 0.1–2.0 MPa. The particle was levitated electrostatically and ignited by a laser. The radiation intensity (or brightness) decreased monotonically with increasing distance away from the particle surface. Glumac et al. [87] measured the flame temperatures of aluminum particles 5–10 μm in diameter in a shock tube in carbon dioxide environments at elevated pressures (>1 atm). The flame temperatures were calculated based on the intensity of the light emitted by the particles. They were in the range of 3000–3100 K, close to the boiling temperature of aluminum at elevated pressures. These results support the idea that combustion of micron-sized aluminum particles in carbon dioxide occur on (or near) the particle surface.

3.2. Flame Temperatures of Nano Aluminum Particles

The actual flame temperatures of nano aluminum particles are significantly lower than the adiabatic counterparts due to heat losses to the ambient gas. Figure 10 shows the measured flame temperatures of aluminum particles in oxygenated gases as a function of the particle size for different pressures and oxygen concentrations [66, 69, 82, 88, 92, 93]. The measurements at 1 atm correspond to laser-ignited particles, and those at higher pressures correspond to shock-ignited particles. The flame temperature is calculated based on the intensity of light emitted by the particles. For micron-sized aluminum particles, the measured flame temperatures are nearly equal to the adiabatic counterparts. For example, at a pressure of 1 atm, the flame temperatures of 210–250- μm particles in air are in the range of 3273–3800 K, around the adiabatic flame temperature of 3500 K [82, 88]. The flame temperature of ≈ 20 - μm particles increases from about 2200 to 3100 K as the

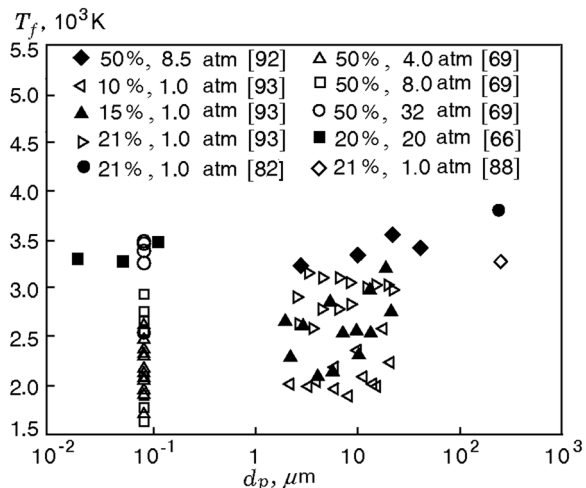


Fig. 10. Measured flame temperatures of aluminum particles as a function of the particle size for different pressures and oxygen concentrations.

oxygen concentration increases from 10 to 21%. This trend agrees with the results of the chemical equilibrium analysis [81]. Note that there is a considerable scatter (as high as 500 K) in the measured flame temperatures [93], but the results do indicate substantial reduction in the flame temperature with decreasing oxygen molar fraction.

For nano aluminum particles, the flame temperature is substantially lower than the ambient gas temperature, especially at lower pressures. For example, for an oxygen concentration of 50%, the measured flame temperatures of 80-nm particles are as low as 1630 K at $p = 8$ atm. The scatter in the measurements can be attributed to the differences in the temperatures of the ambient gases [69], which was varied in the range of 1200–2100 K. The flame temperature increases with increasing pressure and attains a value of 3450 K at $p = 32$ atm. The boiling temperature of aluminum is also a function of pressure, and it takes a value of 3800 K at $p = 32$ atm. Surface reactions are important even for higher pressures in oxygenated environments. The flame temperature of nano aluminum particles is a weak function of the particle size. Further measurements are, however, necessary to ascertain the validity of this trend.

The flame temperature is a size-dependent quantity for other oxidizing gases. Figure 11 shows the measured flame temperatures of aluminum particles as functions of the particle size in carbon dioxide environments for different pressures and oxidizer concentrations [69, 84, 92]. For particle sizes greater than 1 μm , the flame temperature reaches a value of ≈ 3000 K. The data of Yetter and Dryer [84] correspond to pure CO_2 at $p = 1$ atm,

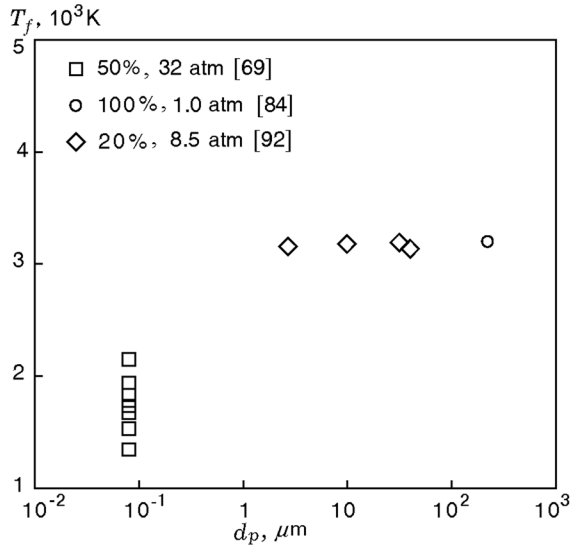


Fig. 11. Measured flame temperatures of aluminum particles as functions of the particle size for different pressures and carbon dioxide concentrations.

while the measurements of Bazyn et al. [69, 92] were obtained for lower oxidizer concentrations of 20 and 50% and higher pressures of 8.5 and 32 atm. The flame temperatures of 80-nm particles vary in the range of 1345–2151 K, depending on the ambient gas temperature. These values are significantly lower than the adiabatic flame temperature and boiling temperature of aluminum. Combustion of nano aluminum particles in carbon dioxide must occur heterogeneously on the particle surface over the pressure range of concern.

It is apparent that heat losses to the ambient gas have a significant effect on the flame temperature of nano aluminum particles. Allen et al. [66] studied combustion of nano aluminum particles with the help of a shock tube in oxygen–nitrogen gas mixtures at a pressure of 20 atm and temperature of 1500 K. The particle size varied in the range of 18–110 nm. The molar concentration of oxygen was 20%. The measured flame temperatures of 80-nm particles in oxygen-containing gases were ≈ 3169 K and 2375 K at 20 and 3.5 atm, respectively. The particle burning time was on the order of 100 μ s. A companion theoretical study was performed, where the burning time and flame temperature were calculated by means of a transient energy balance analysis. The burning rate was assumed to be controlled by collisions of oxidizer molecules on the particle surface. Heat losses to the ambient gas by conduction and radiation were considered. The particle energy conservation equation is written as

$$m_p c_p \frac{dT}{dt} = \dot{Q}_{\text{gen}} - \dot{Q}_{\text{rad}} - \dot{Q}_{\text{cond}}, \quad (14)$$

where m_p is the particle mass. The rate of chemical heat generation is given by the formula

$$\dot{Q}_{\text{gen}} = A_p \varphi N_{\text{ox}} \frac{vq}{4}, \quad (15)$$

where A_p is the particle surface area, φ is the sticking probability, N_{ox} is the number concentration of oxidizer molecules, v is the molecular speed, and q is the heat of the reaction.

The sticking probability refers to the fraction of collisions that result in chemical reactions. The radiation and conduction heat transfer rates are expressed as

$$\dot{Q}_{\text{rad}} = \varepsilon_p k_B A_p (T_p^4 - T_a^4), \quad (16)$$

$$\dot{Q}_{\text{cond}} = \alpha \pi d_p^2 \frac{p_a}{8} \sqrt{\frac{8k_B T_a}{\pi m_a}} \left(\frac{\gamma + 1}{\gamma - 1} \right) \left(\frac{T_p}{T_a} - 1 \right), \quad (17)$$

where ε_p is the emissivity of the particle.

Reasonably good agreement with experimental data was achieved, provided that the accommodation coefficient and sticking probability are taken to be $\alpha = 0.0035$ and $\varphi = 0.0009$, respectively. The former value agrees with the Altman's limit for the energy accommodation coefficient α [94]

$$\alpha < \frac{\theta^2}{[2(c_v/R) + 1]T_a T_p}, \quad (18)$$

where c_v is the molar specific heat of the gas and $\theta = 428$ K is the Debye temperature of aluminum.

The conduction heat transfer rate is proportional to the gas pressure, whereas the radiation counterpart is independent of pressure. As the accommodation coefficient is significantly lower than unity, the actual conduction heat transfer is negligible, compared to the theoretical value under complete energy accommodation. Radiation heat transfer is relatively more significant at nano scales. As a result, the net heat transfer rate is a relatively weak function of the gas pressure. It is, however, apparent from Eq. (15) that the reaction rate is proportional to the gas pressure. Consequently, a higher flame temperature is observed at a greater pressure for nano aluminum particles. The theoretical analysis of Allen et al. [66] explains the pressure dependence of the flame temperature of nano aluminum particles.

3.3. Emission and Absorption Spectrum

Aluminum monoxide (AlO) is an important gas-phase intermediate during combustion of aluminum particles. The presence of AlO is marked by a sharp peak in the emission intensity at a wavelength of around 460–530 nm in the spectrum [66]. AlO is present only in the high-temperature region. The spectral behavior of

AlO emission can, thus, be used to infer the flame temperature. Lynch et al. [76] employed absorption spectroscopy to detect the presence of AlO during combustion of aluminum particles in oxygenated environments in a shock tube. The molar concentration of the oxidizer was 40%, and the pressure of the ambient gas was 7 atm. Two different particle sizes of 2 μm and 80 nm were considered. The gas temperature was decreased from 2400 K in increments of ≈ 100 K until AlO was not seen in the spectrum. AlO was detected down to 2083.4 and 1996 K for micron-sized and nano aluminum particles, respectively. It is well known that the ignition temperatures of nano aluminum particles are as low as 900 K. As a result, most of the experiments on combustion of nano aluminum particles are performed at gas temperatures substantially lower than 2000 K. The results of Lynch et al. [76] clearly suggest that AlO is not present in the majority of experiments on combustion of nano aluminum particles.

Recent studies [66, 69] indicate weak or negligible AlO emission for pressures up to 20 and 32 atm in oxygenated and carbon dioxide environments, respectively. Significant emission from AlO was, however, detected in oxygen-containing gases at $p = 32$ atm (Fig. 12). At a pressure of 32 atm and temperature of 1600 K, the temperature obtained from spectral fitting of the AlO emission intensity is 4159 ± 200 K for the molar concentration of oxygen of 50%. The particle temperature obtained by recording the thermal radiation from the particle by using a pyrometer is ≈ 3500 K. As a result, reactions may occur on (or very close to) the particle surface at the pressure $p = 32$ atm. This is more so at lower pressures. The intensity of light emitted by the particles can be used to obtain the burning time. Figure 13 shows the temporal variation of the intensity of light emitted by 80-nm aluminum particles in a gas consisting of CO₂ (50%) and N₂ (50%) at a temperature of 1760 K and pressure of 32 atm. The burning time is defined as the time period between 10 and 90% of the total integrated emission intensity.

3.4. Heat Transfer Effects on the Flame Standoff Distance

The transition from the continuum to free-molecular heat transfer regime drives the flame closer to the particle surface [95]. Mohan et al. [95] conducted a theoretical analysis of gas-phase combustion of aluminum particles in air, carbon dioxide, and water. The particle was assumed to be surrounded by a gas-phase flame, and the particle temperature was taken to be the boiling point of aluminum. The energy released in the stationary flame zone (\dot{Q}_c) must balance the heat losses to the particle (\dot{Q}_p) and ambient gas (\dot{Q}_a):

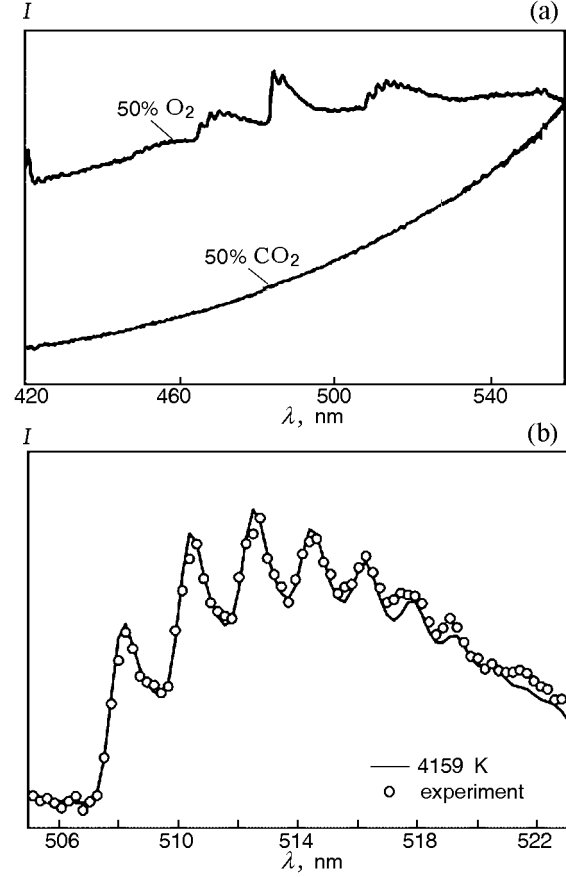


Fig. 12. (a) Emission spectra during combustion of 80-nm aluminum particles in oxygenated and carbon dioxide environments at $p = 32$ atm and $T = 1900$ K; (b) comparisons of the measured and fitted spectra for 80-nm particles in an oxygenated environment at $T = 1600$ K and $p = 32$ atm [69].

$$\dot{Q}_c = \dot{Q}_a + \dot{Q}_p. \quad (19)$$

The gas-phase flame is a spherical surface, and the flame diameter was assumed to be significantly greater than the mean free path of gas molecules. The rate of heat losses from the flame to the ambient gas was expressed as

$$\dot{Q}_a = 2\pi d_f \lambda_a (T_f - T_a), \quad (20)$$

where T_f is the flame temperature.

The rate of heat transfer between the particle and the flame was calculated by using both continuum and free-molecular models:

$$\dot{Q}_{p,\text{cont}} = 2\pi \frac{d_p d_f}{d_f - d_p} \lambda_a (T_f - T_p), \quad (21)$$

$$\dot{Q}_{p,\text{free}} = \frac{\alpha}{8} \pi d_p^2 p_a v \frac{\gamma + 1}{\gamma - 1} \left(1 - \frac{T_p}{T_f} \right). \quad (22)$$

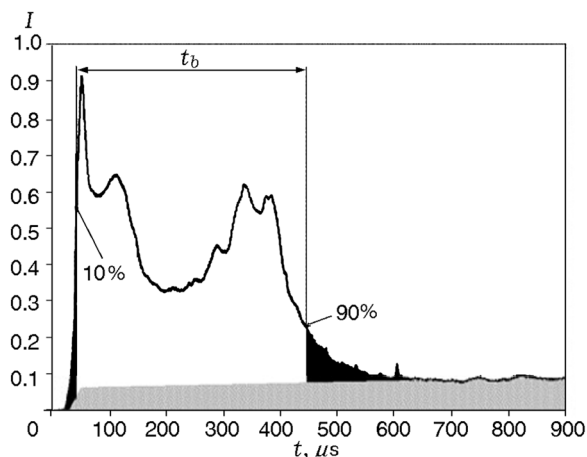


Fig. 13. Temporal variation of the intensity of light emitted by 80-nm aluminum particles in a gas consisting of CO_2 (50%) and N_2 (50%) at $T = 1760$ K and $p = 32$ atm [69]: t_b is the time period between 10 and 90% of the total integrated emission intensity; the background emission is marked by the gray color.

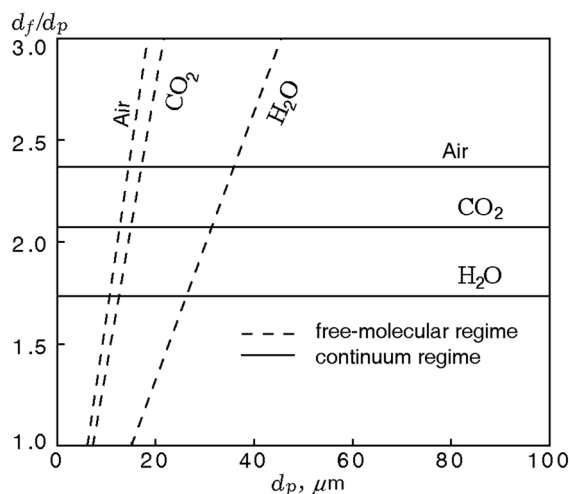


Fig. 14. Effect of the particle size on the maximum value of the flame-to-particle diameter ratio for different oxidizers [95].

The accommodation coefficient was taken to be unity in order to maximize the heat flux to the particle. The vaporization rate of aluminum is controlled by the rate of heat transfer from the flame to the particle surface. As a result, the chemical energy release rate can be written as

$$\dot{Q}_c = \dot{Q}_p \frac{H_r}{L_v}. \quad (23)$$

For a given particle size, a large flame is harder to sustain due to greater heat losses to the ambient gas and reduced heat transfer to the particle. Figure 14 shows

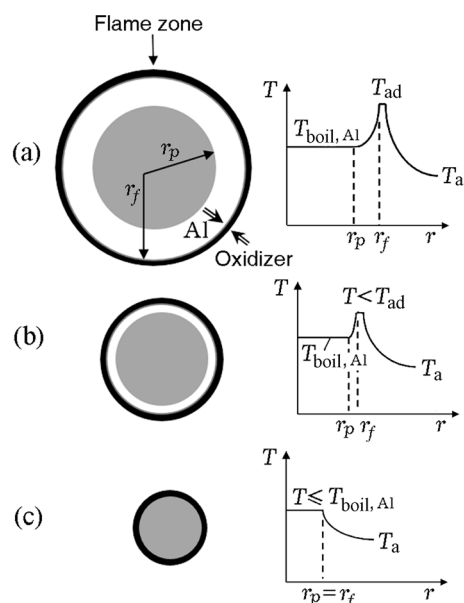


Fig. 15. Flame structures of aluminum particles in air: (a) micron-sized and larger particle (vapor-phase combustion); (b) micron-sized particles (combustion near the particle surface); (c) nanoparticles (surface combustion) [92].

the effect of the particle size on the maximum value of the flame-to-particle diameter ratio ($D = d_f/d_p$) for different oxidizers. The continuum model indicates that the flame is detached from the particle surface, irrespective of the particle size. The calculated flame-to-particle diameter ratio is in the range of 1.5–2.0, which agrees with experimental data. The free-molecular model, on the other hand, suggests that the flame is located closer to the particle surface for smaller particles. The particle size corresponding to $D = 1$ represents the critical value below which the flame is located at the particle surface. The calculated critical particle diameters are 6.1, 7.2, and 15.1 μm for air, carbon dioxide, and water vapor, respectively. The results suggest that combustion of nano aluminum particles occurs heterogeneously on the particle surface regardless of the oxidizing gas.

3.5. Flame Structures of Aluminum Particles

Results of experimental and theoretical studies can be used to hypothesize the flame structure of aluminum particles over a broad range of particle sizes (Fig. 15). For micron-sized and larger particles, a detached gas-phase diffusion flame is formed. The temperature increases with increasing distance away from the particle surface, attains its maximum value in the flame zone, and then gradually decreases to the ambient gas tem-

perature in the far field. The peak temperature is nearly equal to the adiabatic flame temperature of the Al–air system. For smaller particles, surface reactions become important, and the flame front moves closer to the particle surface. The flame temperature can be significantly lower than the adiabatic counterpart due to the effect of heat losses to the ambient gas. For nano aluminum particles, reactions primarily occur on the particle surface. The flame temperature is nearly equal to the ambient gas temperature, especially at low pressures, and typically does not exceed the boiling temperature of aluminum ($T_{\text{boil,Al}}$). The temperature decreases with increasing distance away from the particle surface.

4. PARTICLE BURNING TIME

4.1. Diffusion Regime (Micron-Sized and Larger Particles)

One of the most important parameters that characterize the reactivity of aluminum particles is the single particle burning time. For micron-sized and larger particles, the burning time has a particle size dependence of the form $t = ad_p^n$, where $n = 1.5\text{--}2.0$ [85, 96–101]. The burning time is weakly dependent on the temperature and pressure of the ambient gas [99, 102]. This corroborates the fact that the burning rate is controlled by mass diffusion through the gas-phase mixture. Beckstead [103] assimilated numerous experimental data and obtained the correlation for the single particle burning time

$$t_b = \frac{cd_p^{1.8}}{X_{\text{eff}}p^{0.1}T_0^{0.2}}, \quad (24)$$

where X_{eff} is the effective concentration of the oxidizer, $X_{\text{eff}} = C_{\text{O}_2} + 0.6C_{\text{H}_2\text{O}} + 0.22C_{\text{CO}_2}$, p [atm] is the pressure, T [K] is the initial temperature, d_p [μm] is the particle diameter, and $c = 7.35 \cdot 10^{-6}$ is a constant. Note that Eq. (24) is valid only for micron-sized or larger particles that burn under diffusion-controlled conditions.

4.2. Transition Regime

For particles smaller than 10 μm , the effect of chemical kinetics on the burning time is significant. Bazyn et al. [92] measured the burning times of micron-sized aluminum particles in oxygenated environments in a shock tube. The particle size varied in the range of 3–40 μm , and the pressure range of concern was 3–30 atm. For a 10- μm aluminum particle, the burning time was roughly inversely proportional to the gas pressure. This trend is indicative of the kinetically controlled combustion regime. For diffusion-controlled conditions, the

Table 3. Coefficients in the burning time model for particles in the transition regime

Oxidizer	a_0	a_1	a_2
O ₂	200	0.5	−0.5
CO ₂	500	0.6	0.3
H ₂ O	86	−1.7	0.75

burning time is weakly dependent on the gas pressure. The transition from the diffusion-controlled to kinetically controlled combustion regime was observed to occur at a particle size of 10 μm . Lynch et al. [104] similarly measured the burning times of aluminum particles 3–11 μm in diameter in oxygen, carbon dioxide, and water vapor oxidizers at high temperatures (2400–3000 K). The pressure range of concern was 4–25 atm. The burning time had a particle size dependence of the form $t_b = ad_p^n$, where the exponent n was significantly lower than unity. In oxygenated environments, the burning time was roughly inversely proportional to pressure, which is consistent with the results of Bazyn et al. [92]. For carbon dioxide and water vapor oxidizers, the burning time of aluminum particles increased with increasing pressure. This was attributed to the effects of radical recombination reactions and the pressure dependence of the boiling temperature of aluminum. Further measurements are necessary to ascertain the validity of this trend.

The following correlation was established for the burning time of aluminum particles in the transition regime [104]:

$$t_b = a_0 X_{\text{ox}} \left(\frac{p}{p_0} \right)^{a_2} d_p^n, \quad (25)$$

$$n = 2 \exp(-4.3 X_{\text{ox}}) \left(\frac{p}{p_0} \right)^{-0.3}.$$

Here t_b is the burning time given in microseconds, $p_0 = 8.5$ atm, X_{ox} is the molar fraction of the oxidizer, and d_p is the particle diameter measured in micrometers. The constants are listed in Table 3. The exponent n decreases with increasing oxidizer concentration from ≈ 2.0 at the zero concentration to ≈ 0 at the 100% concentration. For oxygen and carbon dioxide, the burning time is roughly inversely proportional to the square root of the oxidizer concentration. A stronger effect of the oxidizer concentration on the burning time is observed for water vapor. The burning-time pressure exponents are −0.50, 0.30, and 0.75 for oxygen, carbon dioxide, and water vapor, respectively. Note that the diameter exponent is also a function of pressure. Clearly, several aspects of combustion of aluminum particles in the transition regime are not completely understood.

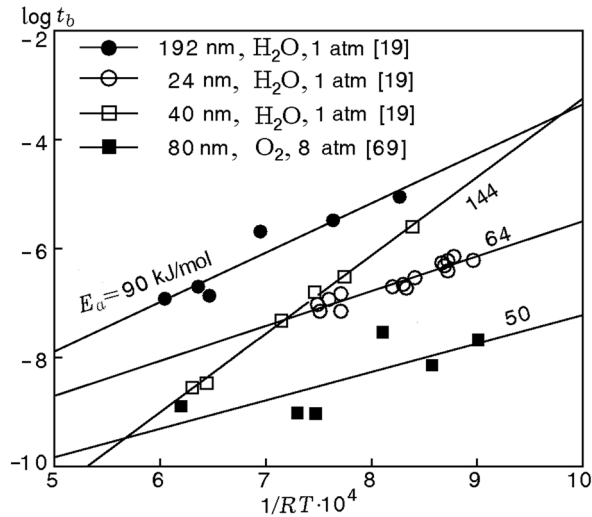


Fig. 16. Variation of the burning time of nano aluminum particles with the ambient gas temperature.

4.3. Kinetic Regime (Nano Aluminum Particles)

Experimental data on the burning times of nano aluminum particles are scarce. The ambient gas temperature has a pronounced effect on the burning properties of nano aluminum particles. Figure 16 shows the effect of the gas temperature on the burning time of nano aluminum particles in water vapor [19] and oxygenated [69] environments. Parr et al. [19] used a hydrogen-oxygen-argon burner. The temperature was controlled by varying the argon concentration, and the particles were introduced into the hydrogen gas flow. Hydrogen and oxygen were fed at the stoichiometric ratio, with water vapor acting as an active oxidizer. The burning time was calculated from the length of the burning region and the gas velocity. Bazyn et al. [69] studied particle combustion in an oxygen-nitrogen gas mixture by employing a shock tube, as discussed in Section 3. The burning time was found to be an exponential function of the gas temperature. The activation energies fall in the range of 50–144 kJ/mol. An unusual trend was observed for the burning time of 80-nm aluminum particles in the carbon dioxide environment. At a pressure of 32 atm, the burning time remained approximately constant ($\approx 400 \mu\text{s}$) up to a temperature of $\approx 2000 \text{ K}$ and then decreased sharply to a value of $\approx 50 \mu\text{s}$ at 2100 K [69]. The visible light intensity signals were, however, affected by changes in the ambient gas temperature, even for temperatures lower than 2000 K.

The particle size exerts a weak effect on the burning time of nano aluminum particles (Fig. 17). The burning time has a size dependence of the form $t_b = ad_p^n$,

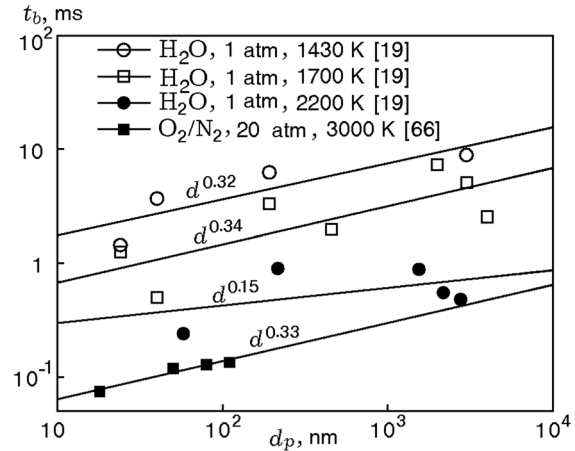


Fig. 17. Effect of the particle size on the burning time of nano aluminum particles with different oxidizers.

where $n = 0.15\text{--}0.34$. The observed trend suggests that the burning behaviors of nano aluminum particles are dictated by chemical kinetics. Note that the diameter exponent is significantly smaller than unity. The phenomenon may be attributed to sintering and agglomeration of particles [105] and/or to the fractal nature of the particle surface [106].

Chakraborty and Zachariah [105] conducted MD simulations and examined sintering of two identical passivated nano aluminum particles. Two different particle sizes of 8 and 16 nm were considered. The oxide layer thickness was 1.5 nm. The particles were heated from 500 to 2000 K at a rate of $10^{13}\text{--}10^{14} \text{ K/s}$, and the temperature was then held constant. The particles sintered completely, despite of the fact that the temperature was lower than the bulk melting point of alumina (2350 K). The oxide shell melted at a lower temperature of 2000 K, possibly, due to diffusion of aluminum atoms and formation of an aluminum sub-oxide, which has different physicochemical properties. Furthermore, it is well known that the melting temperature of the nano-scale oxide shell is substantially lower than the bulk value of 2350 K. For example, Puri and Yang [107] observed melting of an oxide shell 1 nm thick at temperatures as low as 937 K. The time taken for the fusion of two 8-nm particles was calculated to be 0.7 ns, while the reaction time of nano aluminum particles was on the order of 10–100 μs [19, 69]. Consequently, sintering and aggregation of particles are significant during ignition and combustion of aluminum particles. The measured burning times may fail to correspond to the initial particle size.

In conventional models (for example, [66]), it is assumed that oxidizer molecules collide and react on a

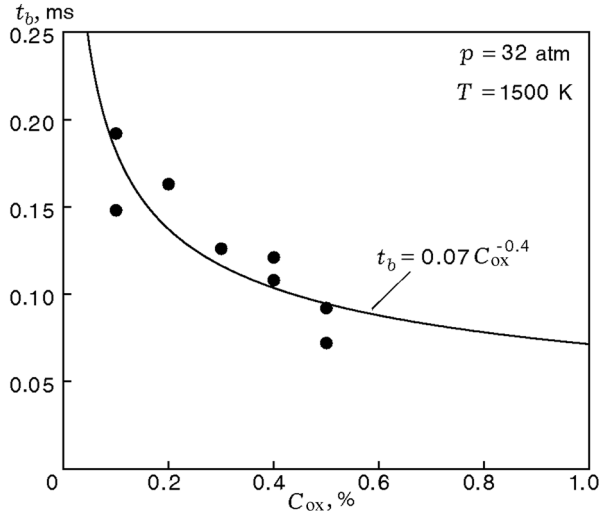


Fig. 18. Effect of the oxygen concentration on the burning time of 80-nm aluminum particles at $p = 32$ atm and $T = 1500$ K [69].

smooth spherical surface of an aluminum particle. In reality, surface roughness and the presence of cracks in the oxide layer [106] may alter the relationship between the particle diameter and the surface area A available for chemical reactions

$$A = A_{\text{ref}} \left(\frac{d_p}{D_{\text{ref}}} \right)^{D_{\text{frac}}}, \quad (26)$$

where the fractal dimension D_{frac} varies in the range of 2–3.

Buckmaster and Jackson [106] conducted a theoretical analysis and studied the effect of cracks in the oxide layer on the burning time of aluminum particles. For kinetically controlled conditions, the particle-size dependence of the burning time is expressed as

$$t_b \sim d_p^{3-D_{\text{frac}}}. \quad (27)$$

For non-fractal surfaces, the burning time is linearly proportional to the particle size. The burning-time diameter exponent decreases from 1 to 0 as the fractal dimension increases from 2 to 3. The weak effect of the particle size on the burning time of nano aluminum particles may stem from the fractal nature of the surface available for chemical reactions.

The oxidizer concentration is yet another parameter that dictates the burning behaviors of aluminum particles. Figure 18 shows the effect of the oxidizer concentration on the burning time of 80-nm particles at a pressure of 32 atm and temperature of 1500 K. The work was conducted by using a shock tube, with the burning time calculated from the temporal variations of the intensity of light emitted by particles. The burning

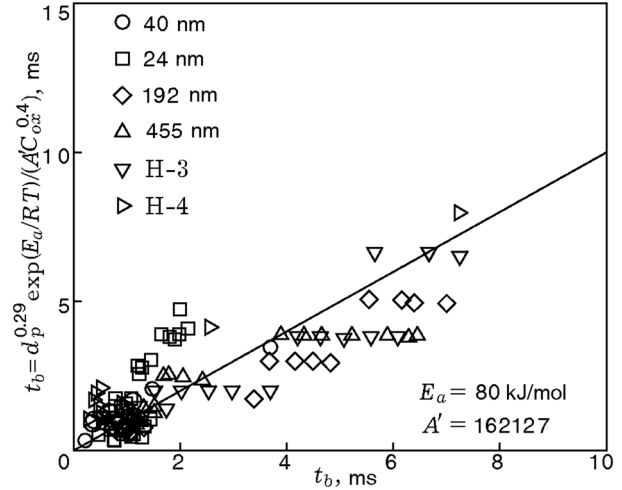


Fig. 19. Measured burning times of nano aluminum particles (points) versus the curve-fitting values (curve) ($\text{H}_2\text{O}/\text{Ar}$, 1 atm [19]).

time exhibits a concentration dependence of the form $t_b = 0.07 C_{\text{ox}}^n$, where $n = -0.4$. The theoretical burning time is inversely proportional to the concentration of the oxidizing gas. The actual concentration effect on the burning time is, thus, weaker than the theoretical counterpart.

Experimental data [19] and [69] are used to obtain the correlation for the burning time of nano aluminum particles at 1 atm:

$$t_b = \frac{d_p^{0.29} \exp(E_a/RT)}{A' C_{\text{ox}}^{0.4}}, \quad (28)$$

where $E_a = 80$ kJ/mol, $A' = 162127$, and d_p is given in micrometers.

Figure 19 shows a comparison of the measured burning times and the curve-fitting values. Reasonably good agreement is obtained, thereby demonstrating the validity of the proposed correlation. Note that the correlation does not consider the effects of pressure and the type of the oxidizer on the burning time, since they are poorly understood.

Bazyn et al. [69] measured the burning times of 80-nm aluminum particles using a shock tube in oxygenated environments at two different pressures of 8 and 32 atm. The results are shown in Fig. 20. At temperatures lower than 1600 K, the burning time decreases by a factor of 3 as the gas pressure increases from 8 to 32 atm. The burning time, however, is a relatively weak function of the gas pressure at temperatures greater than 1600 K. At 8 atm, the measured flame temperatures are strongly dependent on the ambient gas temperature. The flame temperature, on the

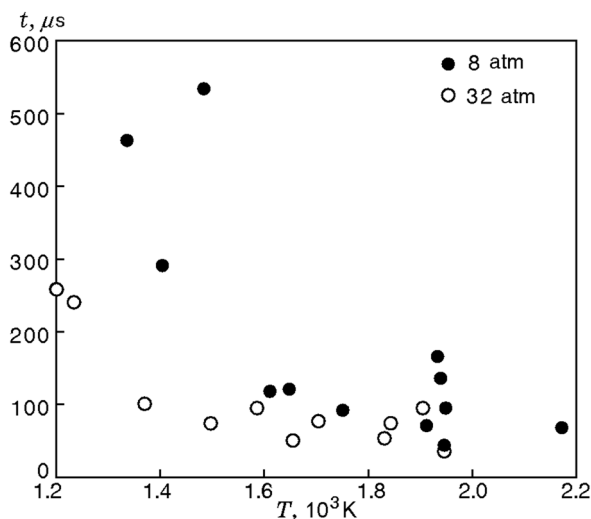


Fig. 20. Effect of pressure on the burning time of 80-nm aluminum particles in an oxygenated environment [69].

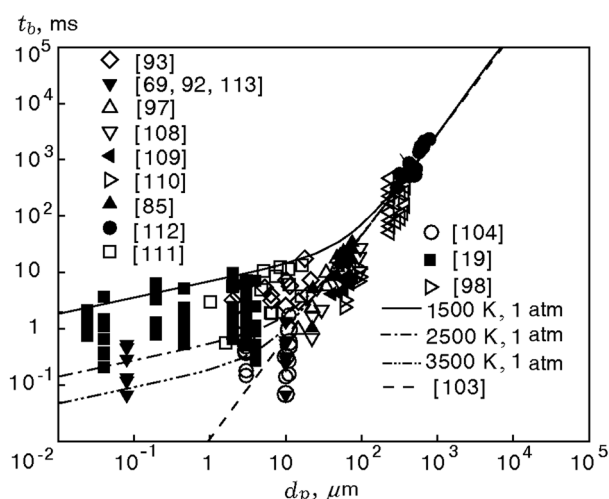


Fig. 21. Comparison of the burning time of aluminum particles obtained by using empirical correlations (curves) with experimental data (points).

other hand, becomes relatively independent of the gas temperature at 32 atm and has a value of ≈ 3500 K. The effect of the type of the oxidizer on the burning time remains unknown. For example, at a pressure of 32 atm and temperature of 1500 K, the burning time of 80-nm particles in carbon dioxide is nearly four times that in oxygenated environments. At temperatures greater than 2000 K, the burning times in oxygen and carbon dioxide are comparable to each other. Further studies are needed to elucidate the effects of the pressure and the oxidizer type on the burning time of nano aluminum particles.

Figure 21 shows the burning time of aluminum particles as a function of the particle size for different oxidizers, temperatures, and pressures. Experimental data from different sources [66, 69, 85, 92, 93, 97, 98, 104, 108–113] are shown. Various empirical correlations are compared with experimental measurements.

As discussed in Section 2.4, the burning behavior of aluminum particles may depend on the heating rate. For heating rates greater than 10^6 K/s, the melt-dispersion mechanism may become operative. A number of studies have been conducted to ascertain the validity of the proposed mechanism. Bockman et al. [114] measured the combustion velocities of Al + MoO₃ thermites for three different aluminum particle sizes of 44, 80, and 121 nm. The packing density was roughly 5–10% of the theoretical maximum density (TMD). The MoO₃ particles had a sheet-like structure, with a length of 1 μ m and thickness of 20 nm. The combustion velocity increased with decreasing particle size and attained a limiting value (1 km/s) at a threshold particle size of 50–110 nm. The melt-dispersion mechanism was later proposed to explain the unusual trend [115]. Ohkura et al. [116] provided the first experimental evidence of the melt-dispersion mechanism. The oxidation mechanism of aluminum particles 60–96 nm in size in air at high heating rates ($\approx 10^6$ K/s) was studied by using a flash ignition method. Transmission electron microscopy (TEM) images suggested the rupture of the oxide shell and the presence of small reacted Al clusters. A more detailed review of various theoretical and experimental studies on the melt-dispersion mechanism can be found in [117]. It is important to note that the melt-dispersion mechanism provides a new basis for the design of nano-energetic materials. According to the conventional diffusion theory, the particle reactivity can be enhanced by decreasing the particle diameter or the oxide layer thickness. The melt-dispersion mechanism suggests that the key parameter is the particle radius-to-shell thickness ratio, which has a threshold value $R/\delta = 19$ [118].

CONCLUSIONS

This paper provides a comprehensive review of the combustion characteristics and burning properties of nano aluminum particles. The validity of the continuum assumption is first examined by comparing the particle size and the mean free path of gas molecules. At nano scales, the continuum assumption breaks down, and the ensuing heat and mass transfer rates are substantially overestimated. The model deficiencies are highlighted. Key physicochemical processes of particle combustion

are identified and their respective time scales are compared to determine the combustion mechanisms for different particle sizes and pressures. For particle diameters greater than a critical value, the burning rate is controlled by mass diffusion through the gas-phase mixture. The critical particle size decreases from 100 to 1 μm , as the pressure increases from 1 to 100 atm. It is possible that combustion of nano aluminum particles is controlled by chemical kinetics over the pressure range of practical concern (1–100 atm). Mass diffusion across the oxide layer of the particle is of concern at temperatures lower than the melting temperature of aluminum. It is likely that the oxide layer fractures during ignition, due to core melting and/or polymorphic phase transformations in the oxide layer. As a result, it does not pose significant diffusion resistance during particle combustion. Further studies are necessary to fully understand the role of the oxide layer during combustion of nano aluminum particles. Further empirical evidence is required to justify other theories, such as the proposed melt-dispersion mechanism.

Experimental data from different sources are gathered to elucidate the effect of the particle size on the flame temperature of aluminum particles. For micron-sized particles, the flame temperatures are approximately equal to those of their adiabatic counterparts. Gas-phase reactions occur in oxygenated environments, whereas surface reactions are more important for water and carbon dioxide. The actual flame temperatures of nano aluminum particles are substantially lower than those of their adiabatic counterparts, due to heat losses to the ambient gas.

Measurements indicate weak or negligible aluminum monoxide (AlO) emission for most cases. It is likely that combustion of nano aluminum particles occurs heterogeneously on (or very close to) the particle surface. The burning time of nano aluminum particles is found to be an exponential function of temperature. The activation energies are in the range of 50–144 kJ/mol. The burning time has a particle size dependence of the form $t_b = ad_p^n$, where the exponent n is in the range of 0.15–0.34, significantly lower than unity.

The gas pressure seems to exert a strong effect on the burning time; the burning time decreases by a factor of 3 as the pressure is quadrupled. These results support the idea that the burning rate of nano aluminum particles is limited by chemical kinetics. The weak effect of the particle size on the burning time may be attributed to sintering and agglomeration of particles and/or to the fractal nature of the particle surface. The effects of the type and concentration of the oxidizer on the burning time are also briefly discussed. A new correla-

tion for the burning time of nano aluminum particles is established: $t_b = (A')^{-1} C_{\text{ox}}^{-0.4} d_p^{0.29} \exp(-E_a/RT)$, where $E_a = 80$ kJ/mol is the activation energy and $A = 162127$.

Although a much newer insight has been gained over the past decade, several outstanding issues remain to be addressed. The ignition mechanism of nano aluminum particles is yet to be understood. It is believed that the oxide layer fractures in the course of ignition of aluminum particles, but it is not clear whether this phenomenon is induced by melting of the aluminum core or by the polymorphic phase transformation in the oxide layer. Experimental data indicate that the flame temperature of nano aluminum particles does not exceed the boiling temperature of aluminum for pressures up to 32 atm. In most practical applications, however, pressures as high as 100 atm are of concern. As a result, measurements of the flame temperature for pressures exceeding 32 atm are desired. The results can be used to assess the possibility of vapor-phase combustion of nano aluminum particles at higher pressures. Furthermore, the effect of the particle size on the flame temperature of nano aluminum particles should be further investigated.

Experimental measurements of the burning times of nano aluminum particles are very scarce. The burning time is weakly dependent on the particle size. Perhaps, because of the fractal nature of the particle surface and/or sintering of particles, the burning time decreases only by a factor of 4 as the particle size decreases from 1 μm to 10 nm. As a result of the weak dependence of the burning time on the particle size, the potential benefits of nano aluminum particles are not fully realized. Further studies are warranted.

The pressure dependence of the burning time of nano aluminum particles also remains to be fully understood. For temperatures lower than 1600 K, the burning time decreases by a factor of 3 as the pressure is quadrupled. At higher temperatures, the pressure exerts a weak effect on the burning time. This issue should be further investigated, especially for water and carbon dioxide. The effect of the oxidizer type on the burning time is also unclear. At a temperature of 1500 K, the burning time of 80-nm aluminum particles in carbon dioxide is nearly four times that in oxygen. At temperatures exceeding 2000 K, the burning times in oxygen and carbon dioxide are comparable to each other. Direct comparisons of the measured burning times of nano aluminum particles in water and oxygen are impossible, because they correspond to different pressures.

Finally, the kinetics of combustion of aluminum particles is still poorly understood. Many of the theoretical studies on nano aluminum combustion treat the

rate constant as an adjustable parameter and/or the burning time as an input parameter. The predictive capabilities of such models are, therefore, limited. Future work must endeavor to establish both a significant bank of experimental data and an in-depth theoretical understanding of the kinetics of aluminum particle combustion in different oxidizing environments, so that a predictive model could be developed.

The authors would like to thank the U.S. Air Force Office of Scientific Research (AFOSR) for their sponsorship of this program under Contract No. FA9550-13-1-0004. The support and encouragement provided by Dr. Mitat A. Birkan is greatly appreciated. This work was also financially supported by the Ministry of Education and Science of the Russian Federation within the framework of the Federal Target Program Agreement No. 14.578.21.0034 (RFMEFI57814X0034).

REFERENCES

1. E. W. Price and R. K. Sigman, "Combustion of Aluminized Solid Propellants," in *AIAA Progress in Aeronautics and Astronautics*, Vol. 185: *Solid Propellant Chemistry, Combustion, and Motor Interior Ballistics*, Eds. by V. Yang, T. B. Brill, and W. Z. Ren (AIAA, New York, 2000), pp. 663–687.
2. M. K. Berner, V. E. Zarko, and M. B. Talawar, "Nanoparticles of Energetic Materials: Synthesis and Properties (Review)," *Fiz. Goreniya Vzryva* **49** (6) 3–30 (2013) [*Combust., Expl., Shock Waves* **49** (6), 625–647 (2013)].
3. J. P. Foote, B. R. Thompson, and J. T. Lineberry, "Combustion of Aluminum with Steam for Underwater Propulsion," in *Advances in Chemical Propulsion*, Ed. by G. D. Roy (CRC Press, 2002), pp. 133–145.
4. P. Brousseau and C. J. Anderson, "Nanomeric Aluminum in Explosives," *Propell., Explos., Pyrotech.* **27** (5), 300–306 (2002).
5. E. Shafirovich, V. Diakov, and A. Varma, "Combustion of Novel Chemical Mixtures for Hydrogen Generation," *Combust. Flame* **144** (1/2), 415–418 (2006).
6. C. L. Yeh and K. K. Kuo, "Ignition and Combustion of Boron Particles," *Prog. Energy Combust. Sci.* **22** (6), 511–541 (1996).
7. G. Young, K. Sullivan, M. R. Zachariah, and K. Yu, "Combustion Characteristics of Boron Nanoparticles," *Combust. Flame* **156** (2), 322–333 (2009).
8. A. Ulas, K. K. Kuo, and C. Gotzmer, "Ignition and Combustion of Boron Particles in Fluorine-Containing Environments," *Combust. Flame* **127** (1-2), 1935–1957 (2001).
9. G. P. Sutton and O. Biblarz, *Rocket Propulsion Elements* (John Wiley and Sons, New York, 2010), p. 517.
10. Y. Huang, G. A. Risha, V. Yang, and R. A. Yetter, "Effect of Particle Size on Combustion of Aluminum Particle Dust in Air," *Combust. Flame* **156** (1), 5–13 (2009).
11. D. S. Sundaram, P. Puri, and V. Yang, "Thermochemical Behavior of Nano-Sized Aluminum-Coated Nickel Particles," *J. Nanopart. Res.* **16**, 1–16 (2014).
12. P. Puri and V. Yang, "Effect of Particle Size on Melting of Aluminum at Nano Scales," *J. Phys. Chem. C* **111** (32), 11776–11783 (2007).
13. J. Eckert, J. C. Holzer, C. C. Ahn, Z. Fu, and W. L. Johnson, "Melting Behavior of Nanocrystalline Aluminum Powders," *Nanostruct. Mater.* **2** (4), 407–413 (1993).
14. S. L. Lai, J. R. A. Carlsson, and L. H. Allen, "Melting Point Depression of Al Clusters Generated During the Early Stages of Film Growth: Nanocalorimetry Measurements," *Appl. Phys. Lett.* **72** (9), 1098–1100 (1998).
15. V. I. Levitas and K. Samani, "Size and Mechanics Effects in Surface-Induced Melting of Nanoparticles," *Nature Commun.* **2**, 1–6 (2011).
16. V. I. Levitas, M. L. Pantoya, G. Chauhan, and I. Rivero, "Effect of the Alumina Shell on the Melting Temperature Depression for Aluminum Nanoparticles," *J. Phys. Chem. C* **113** (32), 14088–14096 (2009).
17. C. Q. Sun, Y. Wang, B. K. Yay, S. Li, H. Huang, and Y. B. Zhang, "Correlation between the Melting Point of a Nanosolid and the Cohesive Energy of a Surface Atom," *J. Phys. Chem. B* **106** (41), 10701–10705 (2002).
18. C. Brossard, A. Ulas, C. L. Yeh, and K. K. Kuo, "Ignition and Combustion of Isolated Aluminium Particles in the Post-Flame Region of a Flat-Flame Burner," in *16th Int. Colloquium on the Dynamics of Explosions and Reactive Systems, Krakow, Poland, 1997*.
19. T. P. Parr, C. Johnson, D. Hanson-Parr, K. Higa, and K. Wilson, "Evaluation of Advanced Fuels for Underwater Propulsion," in *39th JANNAF Combustion Subcommittee Meeting, 2003*.
20. I. G. Assovskiy, O. M. Zhigalina, and V. I. Kolesnikov-Svinarev, "Gravity Effect in Aluminum Droplet Ignition and Combustion," in *Fifth Int. Microgravity Combustion Workshop, Cleveland, 1999*.
21. R. Friedman and A. Macek, "Ignition and Combustion of Aluminium Particles in Hot Ambient Gases," *Combust. Flame* **6**, 9–19 (1962).
22. C. J. Bulian, T. T. Kerr, and Puszynski J. A. "Ignition Studies of Aluminum and Metal Oxide Nanopowders," in *31st Int. Pyrotechnics Seminar, Fort Collins, Colorado, 2004*.
23. M. E. Derevyaga, L. N. Stesik, and E. A. Fedorin, "Ignition and Combustion of Aluminum and Zinc in Air," *Fiz. Goreniya Vzryva* **13** (6), 852–857 (1977) [*Combust., Expl., Shock Waves* **13** (6), 722–726 (1977)].

24. V. A. Ermakov, A. A. Razdobreev, A. I. Skorik, V. V. Pozdeev, and S. S. Smolyakov, "Temperature of Aluminum Particles at the Time of Ignition and Combustion," *Fiz. Goreniya Vzryva* **18** (2), 141–143 (1982) [*Combust., Expl., Shock Waves* **18** (2), 256–257 (1982)].
25. D. K. Kuehl, "Ignition and Combustion of Aluminum and Beryllium," *AIAA J.* **3** (12), 2239–2247 (1965).
26. S. Yuasa, Y. Zhu, and S. Sogo, "Ignition and Combustion of Aluminum in Oxygen/Nitrogen Mixture Streams," *Combust. Flame* **108** (4), 387–390 (1997).
27. M. A. Gurevich, K. I. Lapkina, and E. S. Ozerov, "Limiting Conditions of Ignition of an Aluminum Particle," *Fiz. Goreniya Vzryva* **6** (2), 172–176 (1970).
28. M. Schoenitz, C. Chen, and E. L. Dreizin, "Oxidation of Aluminum Particles in the Presence of Water," *J. Phys. Chem. B* **113** (15), 5136–5140 (2009).
29. T. G. Theofanous, X. Chen, P. Di Piazza, M. Epstein, and H. K. Fauske, "Ignition of Aluminum Droplets Behind Shock Waves in Water," *Phys. Fluids* **6** (11), 3513–3515 (1994).
30. M. A. Trunov, M. Schoenitz, and E. L. Dreizin, "Effect of Polymorphic Phase Transformations in Alumina Layer on Ignition of Aluminum Particles," *Combust. Theory Model.* **10** (4), 603–623 (2006).
31. A. Rai, D. Lee, K. Park, and M. R. Zachariah, "Importance of Phase Change of Aluminum in Oxidation of Aluminum Nanoparticles," *J. Phys. Chem. B* **108** (39), 14793–14795 (2004).
32. H. Tyagi, P. E. Phelan, R. Prasher, R. Peck, T. Lee, J. R. Pacheco, and P. Arentzen, "Increased Hot-Plate Ignition Probability for Nanoparticle-Laden Diesel Fuel," *Nano Lett.* **8** (5), 1410–1416 (2008).
33. Y. Gan and L. Qiao, "Combustion Characteristics of Fuel Droplets with Addition of Nano and Micron-Sized Aluminum Particles," *Combust. Flame* **158** (2), 354–368 (2011).
34. J. L. Sabourin, R. A. Yetter, B. W. Asay, J. M. Lloyd, V. E. Sanders, G. A. Risha, and S. F. Son, "Effect of Nanoaluminum and Fumed Silica Particles on Deflagration and Detonation of Nitromethane," *Propell., Explos., Pyrotech.* **34** (5), 385–393 (2009).
35. R. W. Armstrong, B. Baschung, D. W. Booth, and M. Samirant, "Enhanced Propellant Combustion with Nanoparticles," *Nano Lett.* **3** (2), 253–255 (2003).
36. L. Meda, G. Marra, L. Galfetti, S. Inchingalo, F. Severini, and L. De Luca, "Nano-Composites for Rocket Solid Propellants," *Compos. Sci. Technol.* **65** (5), 769–773 (2005).
37. A. Dokhan, E. W. Price, J. M. Seitzman, and R. K. Sisman, "The Effects of Bimodal Aluminum with Ultrafine Aluminum on the Burning Rates of Solid Propellants," *Proc. Combust. Inst.* **29** (2), 2939–2946 (2002).
38. K. Jayaraman, K. V. Anand, S. R. Chakravarthy, and R. Sarathi, "Effect of Nano-Aluminum in Plateau-Burning and Catalyzed Composite Solid Propellant Combustion," *Combust. Flame* **156** (8), 1662–1673 (2009).
39. M. L. Pantoya and J. J. Granier, "Combustion Behavior of Highly Energetic Thermites: Nano versus Micron Composites," *Propell., Explos., Pyrotech.* **30** (1), 53–62 (2005).
40. M. Schoenitz, T. S. Ward, and E. L. Dreizin, "Fully Dense Nano-Composite Energetic Powders Prepared by Aarrested Reactive Milling," *Proc. Combust. Inst.* **30** (2), 2071–2078 (2005).
41. S. F. Son, B. W. Asay, T. J. Foley, R. A. Yetter, M. H. Wu, and G. A. Risha, "Combustion of Nanoscale Al–MoO₃ Thermite in Microchannels," *J. Propul. Power* **23** (4), 715–721 (2007).
42. M. R. Weismiller, J. Y. Malchi, R. A. Yetter, and T. J. Foley, "Dependence of Flame Propagation on Pressure and Pressurizing Gas for an Al/CuO Nanoscale Thermite," *Proc. Combust. Inst.* **32** (2), 1895–1903 (2009).
43. K. Sullivan and M. R. Zachariah, "Simultaneous Pressure and Optical Measurements of Nanoaluminum Thermites: Investigating the Reaction Mechanism," *J. Propul. Power* **26** (3), 467–472 (2010).
44. R. A. Yetter, G. A. Risha, and S. F. Son, "Metal Particle Combustion and Nanotechnology," *Proc. Combust. Inst.* **32** (2), 1819–1838 (2009).
45. M. R. Weismiller, J. Y. Malchi, J. G. Lee, R. A. Yetter, and T. J. Foley, "Effects of Fuel and Oxidizer Particle Dimensions on the Propagation of Aluminum Containing Thermites," *Proc. Combust. Inst.* **33** (2), 1989–1996 (2011).
46. G. A. Risha, S. F. Son, R. A. Yetter, V. Yang, and B. C. Tappan, "Combustion of Nano-Aluminum and Liquid Water," *Proc. Combust. Inst.* **31** (2), 2029–2036 (2007).
47. G. A. Risha, T. L. Connell, Jr, R. A. Yetter, D. S. Sundaram, and V. Yang, "Combustion of Frozen Nanoaluminum and Water Mixtures," *J. Propul. Power* **30** (1), 133–142 (2014).
48. D. S. Sundaram, V. Yang, T. L. Connell, Jr, G. A. Risha, and R. A. Yetter, "Flame Propagation of Nano/Micron-Sized Aluminum Particles and Ice (AL-ICE) Mixtures," *Proc. Combust. Inst.* **34** (2), 2221–2228 (2013).
49. V. G. Ivanov, O. V. Gavriluyuk, O. V. Glazkov, and M. N. Safronov, "Specific Features of the Reaction between Ultrafine Aluminum and Water in a Combustion Regime," *Fiz. Goreniya Vzryva* **36** (2), 60–66 (2000) [*Combust., Expl., Shock Waves* **36** (2), 213–219 (2000)].
50. E. Shafirovich, V. Diakov, and A. Varma, "Combustion of Novel Chemical Mixtures for Hydrogen Generation," *Combust. Flame* **144** (1/2), 415–418 (2006).
51. M. W. Beckstead, K. Puduppakkam, P. Thakre, and V. Yang, "Modeling of Combustion and Ignition of

- Solid-Propellant Ingredients,” *Prog. Energy Combust. Sci.* **33** (6), 497–551 (2007).
52. T. J. Foley, C. E. Johnson, and K. T. Higa, “Inhibition of Oxide Formation on Aluminum Nanoparticles by Transition Metal Coating,” *Chem. Mater.* **17** (16), 4086–4091 (2005).
 53. R. J. Jouet, A. D. Warren, D. M. Rosenberg, V. J. Bellitto, K. Park, and M. R. Zachariah, “Surface Passivation of Bare Aluminum Nanoparticles using Perfluoroalkyl Carboxylic Acids,” *Chem. Mater.* **17** (11), 2987–2996 (2005).
 54. R. J. Jouet, J. R. Carney, R. H. Granholm, H. W. Sandusky, and A. D. Warren, “Preparation and Reactivity Analysis of Novel Perfluoroalkyl Coated Aluminum Nanocomposites,” *Mater. Sci. Technol.* **22** (4), 422–429 (2006).
 55. Y. Cui, S. Zhao, D. Tao, Z. Liang, D. Huang, and Z. Xu, “Synthesis of Size-Controlled and Discrete Core-Shell Aluminum Nanoparticles with a Wet Chemical Process,” *Mater. Lett.* **121**, 54–57 (2014).
 56. Y. Kwon, A. A. Gromov, and J. I. Strokova, “Passivation of the Surface of Aluminum Nanopowders by Protective Coatings of the Different Chemical Origin,” *Appl. Surface Sci.* **253** (12), 5558–5564 (2007).
 57. D. S. Sundaram, P. Puri, and V. Yang, “Pyrophoricity of Nascent and Passivated Aluminum Particles at Nano-Scales,” *Combust. Flame* **160** (9), 1870–1875 (2013).
 58. A. V. Fedorov and Yu. V. Kharlamova, “Ignition of an Aluminum Particle,” *Fiz. Goreniya Vzryva* **39** (5), 65–68 (2003) [*Combust., Expl., Shock Waves* **39** (5), 544–547 (2003)].
 59. A. V. Fedorov and A. V. Shul’gin, “Point Model of Combustion of Aluminum Nanoparticles in the Reflected Shock Wave,” *Fiz. Goreniya Vzryva* **47** (3), 47–51 (2011) [*Combust., Expl., Shock Waves* **47** (3), 289–293 (2011)].
 60. M. W. Beackstead, Y. Liang, and K. V. Puddupakkam, “Numerical Simulation of Single Aluminum Particle Combustion (Review),” *Fiz. Goreniya Vzryva* **41** (6), 15–33 (2005) [*Combust., Expl., Shock Waves* **41** (6), 622–638 (2005)].
 61. F. Liu, K. J. Daun, D. R. Snelling, and G. J. Smallwood, “Heat Conduction from a Spherical Nanoparticle: Status of Modeling Heat Conduction in Laser-Induced Incandescence,” *Appl. Phys. B* **83** (3), 355–382 (2006).
 62. S. Mohan, M. A. Trunov, and E. L. Dreizin, “Heating and Ignition of Metal Particles in the Transition Heat Transfer Regime,” *J. Heat Transfer* **130** (10), 104505 (2008).
 63. P. Puri, “Multi Scale Modeling of Ignition and Combustion of Micro and Nano Aluminum Particles,” Ph. D. Thesis, Department of Mechanical and Nuclear Engineering (The Pennsylvania State University, University Park, 2008).
 64. A. V. Filippov and D. E. Rosner, “Energy Transfer between an Aerosol Particle and Gas at High Temperature Ratios in the Knudsen Transition Regime,” *Int. J. Heat Mass Transfer.* **43** (1), 127–138 (2000).
 65. A. Ermoline, D. Yildiz, and E. L. Dreizin, “Model of Heterogeneous Combustion of Small Particles,” *Combust. Flame* **160** (12), 2982–2989 (2013).
 66. D. Allen, H. Krier, and N. Glumac, “Heat Transfer Effects in Nano-Aluminum Combustion at High Temperatures,” *Combust. Flame* **161** (1), 295–302 (2014).
 67. O. Levenspiel, *Chemical Reaction Engineering* (John Wiley and Sons, New York, 1962).
 68. T. R. Marrero and E. A. Mason, “Gaseous Diffusion Coefficients,” *J. Phys. Chem. Ref. Data* **1** (1), 3–118 (1972).
 69. T. Bazyn, H. Krier, and N. Glumac, “Combustion of Nanoaluminum at Elevated Pressure and Temperature Behind Reflected Shock Waves,” *Combust. Flame* **145** (4), 703–713 (2006).
 70. K. Park, D. Lee, A. Rai, D. Mukherjee, and M. R. Zachariah, “Size-Resolved Kinetic Measurements of Aluminum Nanoparticle Oxidation with Single Particle Mass Spectrometry,” *J. Phys. Chem. B* **109** (15), 7290–7299 (2005).
 71. B. J. Henz, T. Hawa, and M. R. Zachariah, “On the Role of Built-in Electric Fields on the Ignition of Oxide Coated Nanoaluminum: Ion Mobility Versus Fickian Diffusion,” *J. Appl. Phys.* **107** (2), 024901 (2010).
 72. N. Eisenreich, H. Fietzek, M. Del Mar Juez-Lorenzo, V. Kolarik, A. Koleczko, and V. Weiser, “On the Mechanism of Low Temperature Oxidation for Aluminum Particles Down to the Nano-Scale,” *Propell., Explos., Pyrotech.* **29** (3), 137–145 (2004).
 73. K. Aita, N. Glumac, S. P. Vanka, and H. Krier, “Modeling the Combustion of Nano-Sized Aluminum Particles,” in *44th AIAA Aerospace Sciences Meeting and Exhibit, Reno, Nevada, 2006*.
 74. V. I. Levitas, “Burning Time of Aluminum Nanoparticles: Strong Effect of the Heating Rate and Melt-Dispersion Mechanism,” *Combust. Flame* **156** (2), 543–546 (2009).
 75. V. I. Levitas, M. L. Pantoya, and B. Dikici, “Melt Dispersion Versus Diffusive Oxidation Mechanism for Aluminum Nanoparticles: Critical Experiments and Controlling Parameters,” *Appl. Phys. Lett.* **92** (1), 011921 (2008).
 76. P. Lynch, G. Fiore, H. Krier, and N. Glumac, “Gas-Phase Reaction in Nanoaluminum Combustion,” *Combust. Sci. Technol.* **182** (7), 842–857 (2010).
 77. Y. Li, R. Clark, A. Nakano, R. K. Kalia, and P. Vashishta, “Molecular Dynamics Study of Size Dependence of Combustion of Aluminum Nanoparticles,” *Mater. Res. Soc. Symp. Proc.* (2012).

78. Y. Li, R. K. Kalia, A. Nakano, and P. Vashishta, "Size Effect on the Oxidation of Aluminum Nanoparticle: Multimillion-Atom Reactive Molecular Dynamics Simulations," *J. Appl. Phys.* **114** (13), 134312 (2013).
79. A. V. Grosse and J. B. Conway, "Combustion of Metals in Oxygen," *Ind. Eng. Chem.* **50** (4), 663–672 (1958).
80. I. Glassman, "Combustion of Metals: Physical Considerations. Solid Propellant Rocket Research," in *ARS Progress in Astronautics and Rocketry* (Academic Press, New York, 1960), Vol. 1, pp. 253–258.
81. B. J. McBride and S. Gordon, "Computer Program for Calculation of Complex Chemical Equilibrium Compositions," National Aeronautics and Space Administration (1996).
82. P. Bucher, R. A. Yetter, F. L. Dryer, T. P. Parr, D. M. Hanson-Parr, and E. P. Vicenzi, "Flame Structure Measurement of Single Isolated Aluminum Particles Burning in Air," *Symp. (Int.) on Combustion* **26** (2), 1899–1908 (1996).
83. E. L. Dreizin, "Experimental Study of Stages in Aluminum Particle Combustion in Air," *Combust. Flame* **105** (4), 541–556 (1996).
84. R. A. Yetter and F. L. Dryer, "Metal Particle Combustion and Classification," in *Micro-Gravity Combustion: Fire in Free Fall*, Ed. by H. D. Ross (Academic Press, 2001), pp. 419–478.
85. R. P. Wilson (Jr.), and F. A. Williams, "Experimental Study of the Combustion of Single Aluminum Particles in O₂/Air," *Symp. (Int.) on Combust.* **13** (1), 833–845 (1971).
86. B. Legrand, M. Marion, C. Chauveau, I. Gokalp, and E. Shafirovich, "Ignition and Combustion of Levitated Magnesium and Aluminum Particles in Carbon Dioxide," *Combust. Sci. Technol.* **165** (1), 151–174 (2001).
87. N. Glumac, H. Krier, T. Bazyn, and R. Eyer, "Temperature Measurements of Aluminum Particles Burning in Carbon Dioxide," *Combust. Sci. Technol.* **177** (3), 485–511 (2005).
88. E. L. Dreizin, "On the Mechanism of Asymmetric Aluminum Particle Combustion," *Combust. Flame.* **117** (4), 841–850 (1999).
89. P. Bucher, R. A. Yetter, F. L. Dryer, T. Parr, and D. M. Hanson-Parr, "PLIF Species and Ratiometric Temperature Measurements of Aluminum Particle Combustion in O₂, CO₂ and N₂O Oxidizers and Comparison with Model Calculations," *Symp. (Int.) on Combust.* **27** (2), 2421–2429 (1998).
90. S. Rossi, E. L. Dreizin, and C. K. Law, "Combustion of Aluminum Particles in Carbon Dioxide," *Combust. Sci. Technol.* **164** (1), 209–237 (2001).
91. P. F. Pokhil, A. F. Belyaev, Yu. V. Frolov, V. S. Logachev, and A. I. Korotkov, *Combustion of Powdered Metals in Active Media* (Nauka, Moscow, 1972) [in Russian].
92. T. Bazyn, H. Krier, and N. Glumac, "Evidence for the Transition from the Diffusion-Limit in Aluminum Particle Combustion," *Proc. Combust. Inst.* **31** (2), 2021–2028 (2007).
93. C. Badiola, R. J. Gill, and E. L. Dreizin, "Combustion Characteristics of Micron-Sized Aluminum Particles in Oxygenated Environments," *Combust. Flame* **158** (10), 2064–2070 (2011).
94. I. S. Altman, "On Heat Transfer between Nanoparticles and Gas at High Temperatures," *J. Aerosol Sci.* **30** (1), S423–S424 (1999).
95. S. Mohan, M. A. Trunov, and E. L. Dreizin, "On Possibility of Vapor Phase Combustion for Fine Aluminum Particles," *Combust. Flame* **156** (11), 2213–2216 (2009).
96. A. F. Belyaev, Yu. V. Frolov, and A. I. Korotkov, "On Combustion and Ignition of Fine Aluminum Particles," *Fiz. Goreniya Vzryva* **4** (3), 323–329 (1968).
97. R. Friedman and A. Macek, "Combustion Studies of Single Aluminum Particles," *Symp. (Int.) on Combust.* **9** (1), 703–709 (1963).
98. A. Davis, "Solid Propellants: The Combustion of Particles of Metal Ingredients," *Combust. Flame* **7**, 359–367 (1963).
99. A. Zenin, G. Kusnezov, and V. Kolesnikov, "Physics of Aluminum Particle Combustion at Zero-Gravity," in *AIAA Aerospace Sciences Meeting and Exhibit, Reno, Nevada, 1999*.
100. J. C. Melcher, R. L. Burton, and H. Krier, "Combustion of Aluminum Particles in Solid Rocket Motor Flows," in *AIAA/ASME/SAE/ASEE Joint Propulsion Conference and Exhibit, Los Angeles, 1999*.
101. R. O. Foelsche, R. L. Burton, and H. Krier, "Ignition and Combustion of Aluminum Particles in H₂/O₂/N₂ Combustion Products," *J. Propul. Power* **14** (6), 1001–1008 (1998).
102. M. Marion, C. Chauveau, and I. Gokalp, "Studies on the Ignition and Burning of Levitated Aluminum Particles," *Combust. Sci. Technol.* **115** (4–6), 369–390 (1996).
103. M. W. Beakstead, "Correlating Aluminum Burning Times," *Fiz. Goreniya Vzryva* **41** (5), 55–69 (2005) [*Combust., Expl., Shock Waves* **41** (5), 533–546 (2005)].
104. P. Lynch, H. Krier, and N. Glumac, "A Correlation for Burn time of Aluminum Particles in the Transition Regime," *Proc. Combust. Inst.* **32** (2), 1887–1893 (2009).
105. P. Chakraborty and M. R. Zachariah, "Do Nanoenergetic Particles Remain Nano-Sized during Combustion?" *Combust. Flame* **161** (5), 1408–1416 (2014).
106. J. Buckmaster and T. L. Jackson, "An Examination of the Shrinking-Core Model of Sub-Micron Aluminum

- Combustion,” *Combust. Theory Model.* **17** (2), 335–353 (2013).
107. P. Puri and V. Yang, “Thermo-Mechanical Behavior of Nano Aluminum Particles with Oxide Layers During Melting,” *J. Nanopart. Res.* **12** (8), 2989–3002 (2010).
108. K. O. Hartman, “Ignition and Combustion of Aluminum Particles in Propellant Flame Gases,” in *Proc. of 8th JANNAF Combustion Meeting, 1971*.
109. S. E. Olsen and M. W. Beckstead, “Burn Time Measurements of Single Aluminum Particles in Steam and CO₂ Mixtures,” *J. Propul. Power* **12** (4), 662–671 (1996).
110. J. L. Prentice, “Combustion of Laser-Ignited Aluminum Droplets in Wet and Dry Oxidizers,” in *12th Aerospace Sciences Meeting, Washington, 1974*.
111. R. J. Gill, C. Badiola, and E. L. Dreizin, “Combustion Times and Emission Profiles of Micron-Sized Aluminum Particles Burning in Different Environments,” *Combust. Flame* **157** (11), 2015–2023 (2010).
112. S. C. Wong and S. R. Turns, “Ignition of Aluminum Slurry Droplets,” *Combust. Sci. Technol.* **52** (4-6), 221–242 (1987).
113. T. Bazyn, H. Krier, and N. Glumac, “Oxidizer and Pressure Effects on the Combustion of 10- μ m Aluminum Particles,” *J. Propul. Power* **21** (4), 577–582 (2005).
114. B. Bockmon, M. Pantoya, S. Son, B. Asay, and J. Mang, “Combustion Velocities and Propagation Mechanisms of Metastable Interstitial Composites,” *J. Appl. Phys.* **98**, 064903 (2005).
115. V. I. Levitas, B. W. Asay, S. F. Son, and M. Pantoya, “Melt Dispersion Mechanism for Fast Reaction of Nanothermites,” *Appl. Phys. Lett.* **89**, 071909 (2006).
116. Y. Ohkura, P. M. Rao, and X. Zheng, “Flash Ignition of Al Nanoparticles: Mechanism and Applications,” *Combust. Flame* **158**, 2544–2548 (2011).
117. V. I. Levitas, “Mechanochemical Mechanism for Reaction of Aluminium Nano- and Micrometre-Scale Particles,” *Phil. Trans. Roy Soc. A* **371**, 20120215 (2013).
118. V. I. Levitas, M. L. Pantoya, and B. Dikici, “Melt Dispersion Mechanism Versus Diffusive Oxidation Mechanism for Aluminum Nanoparticles: Critical Experiments and Controlling Parameters,” *Appl. Phys. Lett.* **92**, 011921 (2008).